Edinburgh Research Explorer

Decadal link between longitudinal morphological changes in branching channels of Yangtze Estuary and movement of the offshore depo-center

Decadal link between longitudinal morphological changes in branching channels of Yangtze Estuary and movement of the offshore depo-center

Boyuan Zhu [1]*, Yao Yue [2], Alistair G.L. Borthwick [3], Wenjun Yu [4], Enhang Liang [5], Jinwu Tang [6], Yuanfang Chai [7] and Yitian Li [2]

[1] School of Hydraulic Engineering, Key Laboratory of Water-Sediment Sciences and Water Disaster Prevention of Hunan Province, Changsha University of Science & Technology, Changsha 410114, China

[2] School of Water Resources and Hydropower Engineering, State Key Laboratory of Water Resources and Hydropower Engineering Science, Wuhan University, Wuhan 430072, China

[3] School of Engineering, The University of Edinburgh, The King's Buildings, Edinburgh EH9 3JL, UK

[4] Changjiang Waterway Planning, Design and Research Institute, Wuhan 430040, China

[5] The Key Laboratory of Water and Sediment Sciences，Ministry of Education; College of Environmental Sciences and Engineering，Peking University，Beijing 100871, China

[6] Changjiang Institute of Survey, Planning, Design and Research, Wuhan 430010, China

[7] Department of Earth Sciences, Vrije Universiteit Amsterdam, Amsterdam 1011–1109, Netherlands

17   * Correspondence to: Dr. Boyuan Zhu, School of Hydraulic Engineering, Key Laboratory of Water-Sediment Sciences and Water Disaster

18   Prevention of Hunan Province, Changsha University of Science & Technology, Changsha 410114, China. Email: boyuan@csust.edu.cn

Abstract

In estuaries, the morphology of inland and offshore areas usually evolves synergistically. This study examines the decadal link between longitudinal changes in morphology of branching channels and movement of the offshore depo-center (where sediment deposition rate is maximum) of the Yangtze River estuary, under intense human interference. Integrated data analysis is provided of morphology, runoff discharge, and ebb partition ratio from 1950 to 2017. Channel-volume reductions and change rates between isobaths in branching channels reflect the impact of estuarine engineering projects. Ebb partition ratio and duration of discharge $\geq 60,000$ m^3 s^{-1} act as proxies for the water excavating force in branching channels and runoff intensity. It is found that deposition occurs in the lower/upper sub-reaches (or further downstream/upstream channels) of the inland north/south branching channels, and the offshore depo-center moves southward or southeastward, as runoff intensity grows; the reverse occurs as runoff intensity declines. This is because the horizontal circumfluence in the Yangtze Estuary rotates clockwise as ebb partition ratios of the north/south branching channels increase/decrease for increasing runoff, and conversely rotates anticlockwise for decreasing runoff. Land reclamation activities, the Deepwater Channel Project, and the Qingcaosha Reservoir have impacted greatly on longitudinal changes of morphology in the North Branch and the South Passage and on ebb partition ratio variations in the North/South Channel and the North/South Passage. Dam-induced runoff flattening has enhanced deposition in the upper/lower sub-reaches of the north/south branching channels and caused northward movement of the offshore depo-center, except in areas affected by estuarine engineering projects. Dam-induced longitudinal evolution of branching channel morphology and offshore depo-center movement will likely persist in the future, given the ongoing construction of large cascade dams in the upper Yangtze and the completion of major projects in the Yangtze Estuary.

Introduction

Morphological changes in estuarine systems directly affect flood risk, navigability, and the aquatic environment, and are impacted by anthropogenic activities, such as dams, flood protection works, and dredging (Dai *et al.*, 2013; Marriner *et al.*, 2013; Robert，2017; Siverd *et al.*, 2018).

Studies of the morphological evolution of coastal regions have tended to examine natural processes at millennial or centurial time scales and anthropogenic progresses at smaller time scales ranging from decades to seasons. The former processes often involve historical sedimentary facies covering vast coastal zones or forming courses of modern estuarine networks (Chen et al., 1982; Stanley & Warne, 1993; Baek et al., 2017). Specific investigations have focused on the evolution of depo-centers (defined as local maxima of the sediment deposition rate) on continental shelves (Fletcher *et al.*, 1992; Nizou *et al.*, 2010; Hanebuth *et al.*, 2015). By combining geological, geographical, and sedimentological perspectives, these researches have revealed the long-term effects of sea level rise, land-surface subsidence, and terrestrial inputs on estuary evolution and depo-center behavior. The latter processes are usually related to local erosion or deposition in estuarine systems, and are caused by variations in sediment load, runoff discharge, and local hydrodynamics due to human interference. For example, reduction in fluvial sediment load due to the trapping effect of river dams has led to widespread recession of river deltas around the world (Rao *et al.*, 2010; Maloney *et al.*, 2018; Zhu CY *et al.*, 2019), whereas runoff regulation of river dams has triggered depositional features (Frihy and Lawrence, 2004; Zamora *et al.*, 2013) and altered spatial erosion-deposition distributions in estuaries (Zhu BY *et al.*, 2017; Zhou *et al.*, 2018). Moreover, estuarine engineering

projects interfere with local hydrodynamics and adjust nearby erosion-deposition patterns (Nitsche *et al.*, 2007; Liu *et al.*, 2009; Luan *et al.*, 2016; El Jakani *et al.*, 2019). The foregoing studies considered the evolution of estuarine areas in the modern period after estuarine systems formed and stabilized, and examined decadal to seasonal impacts of human interference on river/estuary dynamics, sediment movement, and river/estuary bed evolution.

Nowadays, in many estuaries, anthropogenic impacts are larger than natural changes, and so the influence of human activities on the morphological evolution of estuarine systems warrants continuous attention. Therefore, it is necessary first to explore decadal to seasonal morphological changes in offshore and continental areas, which are dominated by natural processes, often accompanied by ancient migratory patterns of estuaries, over very long time scales lasting centuries or even millennia (Chen *et al.*, 1982; Fletcher *et al.*, 1992; Stanley & Warne, 1993; Nizou *et al.*, 2010; Hanebuth *et al.*, 2015; Baek *et al.*, 2017). The movements of offshore depo-centers, located in areas of high deposition rate, cause basic changes in regional erosion-deposition patterns (Fletcher *et al.*, 1992; Nizou *et al.*, 2010; Hanebuth *et al.*, 2015). Consequently, offshore depo-centers are useful indicators of offshore and continental evolution processes. Although researchers have investigated decadal to seasonal morphological changes caused by human disturbances within inland and near-mouth areas (Frihy & Lawrence, 2004; Nitsche *et al.*, 2007; Rao *et al.*, 2010; Zamora *et al.*, 2013; Luan *et al.*, 2016; Zhu BY *et al.*, 2017; Maloney *et al.*, 2018; Zhou *et al.*, 2018; El Jakani *et al.*, 2019; Zhu CY *et al.*, 2019), longitudinal erosion-deposition patterns within inland estuarine channels (i.e., differences in morphological behavior between upper and lower sub-reaches of the channels) have not been systematically studied to date. Furthermore, longitudinal morphological changes within inland channels and depo-center migrations in offshore areas are likely to be associated with each other because of interactions between fluvial and marine hydrodynamics (Yankovsky *et al.*, 2001; Cai *et al.*, 2014; Lee *et al.*, 2017). Insight into the link between longitudinal

morphological changes within inland channels and offshore depo-center movements at decadal to seasonal time scales is therefore necessary for exploring estuaries as integrated systems.

The Yangtze River is the largest river on the Eurasian continent and the third longest river in the world (Yang *et al.*, 2015), with an expansive, bifurcated estuary at its distal end (Yun, 2004). Over past decades, more than 50,000 dams have been constructed and a large number of local engineering projects undertaken in the river basin and its estuary. Surveys have comprehensively examined decadal to seasonal erosion-deposition processes affecting geomorphic units within estuarine and offshore areas of the Yangtze subject to significant variations in water dynamics and sediment supply caused by intense human activities (Liu *et al.*, 2009; Yang *et al.*, 2011; Dai *et al.*, 2013, 2014, 2016; Du *et al.*, 2016; Luan *et al.*, 2016; Yang *et al.*, 2016; Mei *et al.*, 2018; Zhu CY *et al.*, 2019; Zhu BY *et al.*, 2017, 2020). It has been established that certain of these morphological changes have led to practical problems, including migration of navigation features (Liu *et al.*, 2009; Dai *et al.*, 2013), increased risk of embankment failure related to water abstraction projects (Ou *et al.*, 2013), and recession of saltmarsh-wetland systems (Wei *et al.*, 2015; Gu *et al.*, 2018). Nonetheless, there remains a lack of systematic research on the longitudinal changes of morphology in the branching channels of the Yangtze. Meanwhile, recent studies of the decadal movement of the offshore depo-center beyond the river mouth have arrived at dissimilar conclusions. Dai *et al.* (2014) found that the depo-center moved towards the opening of the estuarine channel with highest partition of sediment load. Luan *et al.* (2016) observed that human activities were having an increasingly significant impact. Other researchers reported that the depo-center tended to move southward due to the southeastward self-extension of the Yangtze Delta and engineering-induced strengthening of the seaward flow in south branching channels (Liu *et al.*, 2010; Li *et al.*, 2011; Xu *et al.*, 2013; Yang *et al.*, 2016). These disagreements may have derived from differences in the observed data periods and locations considered. An acceptable scientific explanation is therefore required of

the driving mechanism behind the decadal movement of the offshore depo-center. Improved understanding is also needed of the decadal link between longitudinal erosion-deposition patterns within the inland branching channels and movement of the offshore depo-center. Such understanding requires knowledge of spatial differences in hydrodynamics among the branching channels (Li *et al.*, 2010; Zhu BY *et al.*, 2017) and the concomitant impact on the seaward hydrodynamic field beyond the estuary mouth (Yan *et al.*, 2007; Shen & Li, 2011; Zhang WY *et al.*, 2016).

The present case study explores the longitudinal change of morphology in branching channels of the Yangtze Estuary, the movement of its offshore depo-center, and the connection between these processes at decadal time scale. This is achieved through an integrated analysis of terrain and hydrodynamic data from 1950 to 2017, from which we discern the mechanism behind the general morphological changes and the impact of estuarine engineering projects. Future trends in morphological evolution of inland and offshore areas are predicted from analyses of historical trends and predicted future changes in hydrodynamics. The results should be useful for managing shipping conditions, land resources, and the salt marsh ecosystem of the Yangtze Estuary, which is close to Shanghai and forms part of Jiangsu Province, China. The findings are applicable to other estuarine systems also experiencing channel evolution and depo-center migration under highly variable hydrodynamic conditions.

Study area

The Yangtze Estuary is located at the convergence zone of the Yangtze River and the East China Sea. The estuary is of length of 180 km from west to east and has width of 6-90 km from north to south (Figure 1a-b). It undergoes four major bifurcations at Chongming Island, Baimao Shoal, Changxing Island, Hengsha Island and Jiuduan Shoal, where the channel splits into eight major branches named North Branch, South Branch, North Waterway, South Waterway, North Channel, South channel, North Passage, and South Passage (Figure 1b). The branching

104   network is sketched in Figure 1c.

105   The Yangtze River basin supplies huge annual water discharge and sediment load to the estuary, as recorded at the final downstream, main

106   stem hydrological station at Datong (Luan *et al.*, 2016; Zhu BY *et al.*, 2017; Zhao *et al.*, 2018). Datong holds long-term data on river flux and is

107   located about 500 km upstream of the estuary, with no major tributary or water abstraction works between the station and the upper entrance of

108   the estuary at Xuliujing (Figure 1a-b). More than 50,000 dams have been constructed in the watershed, causing the annual sediment load to

109   decrease sharply and the seasonal distribution of runoff discharge to be flattened significantly, even though the annual runoff discharge has

110   remained almost unchanged (Yang *et al.*, 2011; Luan *et al.*, 2016; Zhang M *et al.*, 2016; Zhu BY *et al.*, 2017). The annual average runoff discharge

111   was about 8960 m^3 yr^{-1} from 1950 to 2017, whereas the annual average river sediment load was 4.25×10^8 t yr^{-1} during 1951-2002 (i.e. pre-TGD

112   period, Figure 1a) and 1.37×10^8 t yr^{-1} during 2003-2017 (i.e. post-TGD period, Figure 1a) (CWRC, 2017).

113   The estuary is meso-tidal with a multi-year average tidal range of 2-3 m (Li *et al.*, 2011; Zhang M *et al.*, 2016); the tidal force at the sea

114   boundary is relatively stable at the yearly time scale (Jiang *et al.*, 2012; Dai *et al.*, 2016; Zhu BY *et al.*, 2017) and drives an enormous yearly flood

115   tidal flow, approximately 9 times larger than the river discharge, into the estuarine zone (Chen & Li, 2002). The entire North Branch (Figure 1b)

116   altered from an ebb-dominated to a flood-dominated channel after the 1950s (Dai *et al.*, 2016; Zhu BY *et al.*, 2017), with the area south of

117   Chongming Island (Figure 1b) experiencing a more complicated hydrodynamic field (dominant ebb-tide between Xuliujing and Hengsha Island

118   (Figure 1b) due to the noteworthy impact of changes in runoff discharge, and migration of the tide reversal interface (where ebb dominance equals

119   flood dominance) from Hengsha Island to the river mouth (Figure 1b) driven by changes in runoff intensity (Shen & Li, 2011; Luan *et al.*, 2016; Han

120   & Huang, 2018)). In the reach downstream of the tide reversal interface, the flood-tide predominates. Given the supply of abundant sediment from

adjacent coastal areas and submerged delta (including the continental shelf), the Yangtze Estuary experiences alternating net exports and imports of sediment (i.e. erosion and deposition events) under alternating high and low runoff discharges, even though the river sediment load has reduced remarkably (Zhu BY *et al.*, 2020).

To exploit available water, land, and shipping resources, several major engineering projects have been implemented in the estuarine area, including the freshwater Qingcaosha Reservoir near Qingcao Shoal, land reclamation along the North Branch, and the Deepwater Channel Project in the North Passage (Figure 1b).

Materials and methods

Data sources

The Changjiang Water Resources Commission provided observed daily water discharge time series at Datong from 1950 to 2017. Nanjing Normal University, Changjiang Water Resources Commission, Shanghai Estuarine & Coastal Science Research Center and Changjiang Waterway Bureau supplied bed-elevation point data digitized from navigational charts determined from 1978 to 2013 surveys. East China Normal University provided data on land reclamation areas along the North Branch. Additional data on hydrodynamic and morphological indexes gathered from published literature comprised: (1) ebb partition ratios for the inland branching channels from 1958 to 2015; (2) locations of the sedimentary body in the North Passage and the offshore depo-center from 1958 to 2015; (3) channel volumes below the 0 m isobath for sub-reaches A, B and C in the North Branch from 1986 to 2013; (4) riverbed erosion/deposition rates for sub-reaches D, E and F in the South Branch from 1958-1973 to 2010-2016 and for sub-reaches G and H in the South Channel from 1997-2001 to 2006-2011; and (5) mean water depths of cross-sections 1-1′, 2-2′ and 3-3′ in the North Channel from 1977 to 2013 and of cross-sections 4-4′, 5-5′ and 6-6′ in the South Passage from 2002 to 2013. Table SI

138 summarizes the data sources.

Processing of morphology

Bed-elevation point data

141 Navigational charts containing bed-elevation point data were digitized for periods from early May or early June to the end of July. Automatic

142 transfer onto Beijing 54 coordinates was conducted using ArcGIS 10.2 with reference to the theoretical low-tide datum at Wusong (Figure 1b). Bed

143 elevations and point locations were based on measurements using dual-frequency echo sounders and GPS positioning. Measurement errors

144 were ±0.1 m for bed-elevation and ±1 m for location; these values are acceptable noting that bed elevation changes can be huge over the yearly

145 time scale (Luan *et al.*, 2016). The sampling density of 3 to 137 pts km^{-2} (i.e. 0.1 to 0.6 km between any pair of adjacent points) resolved spatial

146 variations in terrain, given that bathymetric changes in the Yangtze Estuary are usually gradual over many km (Wang *et al.*, 2008). Thus, a fine

147 grid resolution of 100 m × 200 m was adopted to calculate bathymetric changes and channel volumes by means of Kriging interpolation.

Longitudinal change of channel morphology and depo-center movement

149 The longitudinal change of morphology within inland branching channels was tracked by following variations in riverbed erosion/deposition

150 rates in the upper and lower sub-reaches (Figure 2). Changes to other parameters of interest, such as the sub-reach channel volume and

151 cross-sectional mean water depth, were also used to characterize the longitudinal erosion-deposition patterns in the channels.

152 The offshore depo-center is defined as the location where the sediment deposition rate is a maximum (Figure 2). Herein, northward or

153 southward migration of the offshore depo-center was determined from changes in riverbed erosion/deposition rates in the north and south offshore

154 subareas.

Contributions of boundary change and sedimentation to morphology of the North Branch

Since 1958, land reclamation along the North Branch (Figure 1b; Figure 3) has significantly narrowed the river channel, reducing its volume (Dai *et al.*, 2016). To quantify the contributions of land reclamation and natural sediment deposition to morphological change of the North Branch, we used the following procedure to evaluate the component reductions in channel volume caused by these two factors.

First, channel volumes were calculated below the 0 m isobath, according to the locations of the river boundaries, for two selected years. Then, the total reduction in channel water volume below the 0 m isobath between the two years of interest, ΔV_T (m³), was determined from:

$$\Delta V_T = V_F - V_S \tag{1}$$

where V_F (m³) and V_S (m³) are channel water volumes below the 0 m isobath for the first and second years under consideration.

Second, the constrained channel volume was calculated as the water volume below the 0 m isobath for the first year that fitted within the channel's area of overlap for the two years of interest (obtained by comparing the two river boundaries), V_C (m³). The channel volume reduction caused by the changing river boundary in the time interval between the two years of interest was obtained from:

$$\Delta V_B = V_F - V_C \tag{2}$$

Next, the channel volume reduction below the 0 m isobath caused by natural sediment deposition between the two years of interest, ΔV_N (m³), was computed from:

$$\Delta V_N = \Delta V_T - \Delta V_B \tag{3}$$

Finally, the percentage contributions from boundary change (i.e. land reclamation), C_B (%), and natural sediment deposition, C_N (%), to morphological change of the North Branch in the period of interest were estimated from:

$$C_B = \frac{\Delta V_B}{\Delta V_T} \times 100\% \qquad\qquad (4)$$

and

$$C_N = \frac{\Delta V_N}{\Delta V_T} \times 100\% \qquad\qquad (5)$$

Vertical impact of estuarine engineering projects in branching channels

To identify the vertical impacts of land reclamation in the North Branch and the Deepwater Channel Project in the North Passage (see Figure 1b), we calculated channel volume change rates between adjacent isobaths 1 m apart. The steps were as follows. First, channel volumes below the two adjacent isobaths in the channels were calculated at the start and end of a given time interval. The channel volume change rate between the adjacent isobaths was then evaluated by dividing the difference in channel volume by the time interval. Using this approach, the vertical impact of engineering projects was determined by interpreting the vertical profile of the channel volume change rate in zones close to the projects.

Definition of ebb partition ratio

According to existing theory (Dou, 1964), the morphological evolution of estuarine channels mainly depends on the ebb tidal discharge, which consists of runoff and flood tidal discharge components. In the Yangtze Estuary, both the runoff discharge from the river basin and the flood tidal discharge from the oceanic area remain almost steady at the yearly time scale (Jiang *et al.*, 2012; Dai *et al.*, 2016; Luan *et al.*, 2016; Zhu BY *et al.*, 2017), stabilizing the yearly ebb tidal discharge (Zhu BY *et al.*, 2017). Thus, allocation of yearly (or multi-year average) ebb tidal discharge among the Yangtze estuarine branching channels was determined as the yearly (or multi-year average) ebb partition ratio, η_{ij} (%), defined as follows:

$$187 \qquad \eta_{ij} = \frac{Q_{ij}}{\sum\limits_{j} Q_{ij}} \qquad\qquad (6)$$

188   where Q_{ij} (m^3 s^{-1}) is the yearly (or multi-year average) ebb tidal discharge of the j-th branching channel in the i-th bifurcation of the Yangtze Estuary

189   (Figure 1c). Here, i = 1, …, 4 and j = 1, 2.

Indicator of runoff intensity

191   The multi-year average peak-flood discharge from 1950 to 2017 at Datong was 58,600 m^3 s^{-1}, a value close to the bed-forming discharge of

192   60,400 m^3 s^{-1} in the Yangtze Estuary and thus driving substantial changes to the riverbed (Yun, 2004; Luan et $al.$, 2016). We therefore counted the

193   number of multi-year average duration days for which the runoff discharge exceeded or equaled 60,000 m^3 s^{-1} (thereafter $D_{\geq 60,000}$) during the

194   periods of interest from 1950 to 2017, based on the time series of daily water discharge at Datong. This enabled assessment of the severity of

195   fluvial flood events during these periods. Multi-year average duration days of different runoff discharge levels (at intervals of 10,000 m^3 s^{-1}) were

196   also calculated to examine the variation in intra-annual distribution of runoff discharge.

Results

Longitudinal changes in morphology, corresponding ebb partition ratios, and runoff intensities

199   Table I shows that riverbed erosion/deposition rates in the majority of branching channels (excluding the North Branch and the South Passage)

200   follow a physical law according to variations in multi-year average ebb partition ratios and $D_{\geq 60,000}$. That is, for the north branching channel of each

201   bifurcation, the riverbed deposition rate in the upper/lower sub-reach decreased/increased,   as the multi-year average ebb partition ratio and

202    $D_{\geq 60,000}$ rose. Conversely, the riverbed deposition rate in the upper/lower sub-reach increased/decreased as the multi-year average ebb partition

203 ratio and $D_{\geq 60,000}$ lowered. By comparison, the situation in the south branching channel of each bifurcation was roughly the reverse. The details are

204 as follows:

The South Branch of the first bifurcation

206 Although both the upper and lower sub-reaches of the South Branch experienced erosion during the flood period of 1997-2002, associated

207 with a high value of $D_{\geq 60,000}$ (29 days yr^{-1}), deposition mainly occurred in the lower sub-reach when both sub-reaches underwent deposition during

208 the subsequent dry period of 2002-2007, associated with a low value of $D_{\geq 60,000}$ (4 days yr^{-1}). More severe deposition in the lower sub-reach during

209 the dry period corresponded to a higher value of multi-year average ebb partition ratio in the South Branch.

The second bifurcation

211 For the North Waterway of Baimao Shoal, deposition in the upper sub-reach was larger than that in the lower sub-reach during all four periods

212 of interest. Furthermore, erosion was most severe in the lower sub-reach, with the largest difference in erosion and deposition between the two

213 sub-reaches occurring during the driest period of 2003-2007, corresponding to the lowest value of $D_{\geq 60,000}$ (0 days yr^{-1}). This indicated that more

214 sediment tended to deposit in the upper sub-reach during this period than in any of the other three periods, 1992-1999, 1999-2003, and

215 2007-2010 (which had high values of $D_{\geq 60,000}$ of 31 days yr^{-1}, 15 days yr^{-1} and 9 days yr^{-1}).

216 Upper and lower sub-reaches of the South Waterway of Baimao Shoal suffered erosion and deposition respectively during 1992-1999 and

217 1999-2003 (with high values of $D_{\geq 60,000}$ of 31 days yr^{-1} and 15 days yr^{-1}), whereas both sub-reaches experienced erosion during 2003-2007 and

218 2007-2010 (with low values of $D_{\geq 60,000}$ of 0 days yr^{-1} and 9 days yr^{-1}), indicating that sediment was transported further downstream and deposited

219 in the channel downstream of the South Waterway during these two periods. The lower sub-reach of the South Waterway underwent the largest

220 riverbed deposition rate during the period of 1992-1999 (with a peak value of $D_{\geq 60,000}$ of 31 days yr^{-1}), suggesting substantial upstream sediment

221 transport occurred from the downstream channel into the lower sub-reach of the South Waterway. However, the lower sub-reach and the whole

222 South Waterway experienced the greatest rates of riverbed erosion during 2003-2007, associated with the lowest value of $D_{\geq 60,000}$ (0 days yr^{-1}),

223 implying significant downstream sediment transport from the South Waterway into the downstream channel.

224 Due to data limitations, it was not possible to quantify objectively the change law for the multi-year average ebb partition ratios of the North

225 Waterway and the South Waterway during the four periods of interest.

226 **The third bifurcation**

227 Both the upper and lower sub-reaches of the North Channel experienced erosion during the flood period of 1997-2002 (with a high value of

228 $D_{\geq 60,000}$ of 29 days yr^{-1}), suggesting that sediment was mainly deposited offshore of the North Channel. The upper sub-reach eroded more than the

229 lower sub-reach during this flood period. Both sub-reaches underwent deposition during the dry period of 2002-2007 (with a low value of $D_{\geq 60,000}$ of

230 4 days yr^{-1}), and there was more deposition in the lower sub-reach than the upper sub-reach, implying that sediment was transported upstream

231 from the offshore area into the lower sub-reach of the North Channel during this period. In addition, the multi-year average ebb partition ratio of the

232 North Channel was larger during the flood period of 1997-2002 than that during the dry period of 2002-2007.

233 In the South Channel, both the upper and lower sub-reaches experienced erosion during 1997-2002 and 2002-2007, suggesting that

234 sediment was mainly deposited in the channel downstream of the South Channel during these periods. However, greater erosion occurred in the

235 lower sub-reach than the upper sub-reach during the flood period of 1997-2002 (with a high value of $D_{\geq 60,000}$ of 29 days yr^{-1}), whereas the upper

236 sub-reach witnessed more erosion than the lower sub-reach during the dry period of 2002-2007 (with a low value of $D_{\geq 60,000}$ of 4 days yr^{-1}). This

237 implies downstream transport of sediment from the former flood period to the latter dry period. Moreover, the multi-year average ebb partition ratio

238 of the South Channel was larger during the dry period of 2002-2007 than that during the flood period of 1997-2002.

239 **The North Passage of the fourth bifurcation**

240 During the flood period of 1997-2002, the upper and lower sub-reaches of the North Passage experienced erosion and deposition

241 respectively (with a high value of $D_{\geq 60,000}$ of 29 days yr^{-1}), indicating that sediment was mainly deposited in the lower sub-reach during this period.

242 Both sub-reaches underwent deposition, with more occurring in the upper sub-reach, during the dry periods that followed in 2002-2006 and

243 2006-2007 (associated with low values of $D_{\geq 60,000}$ of 4 days yr^{-1} and 0 days yr^{-1}), implying that sediment was transported upstream into the upper

244 sub-reach during these two dry periods. Both sub-reaches suffered erosion, with the lower sub-reach experiencing more, during the dry period of

245 2007-2009 (corresponding to a low value of $D_{\geq 60,000}$ of 0 days yr^{-1}). This suggests that sediment was transported further upriver in the channel

246 upstream of the North Passage during this period. The multi-year average ebb partition ratio of the North Passage was larger during the flood

247 period of 1997-2002 (with a high value of $D_{\geq 60,000}$ of 29 days yr^{-1}) than during the dry periods of 2002-2006, 2006-2007, and 2007-2009 (which had

248 low $D_{\geq 60,000}$ values of 4 days yr^{-1}, 0 days yr^{-1}, and 0 days yr^{-1}).

249 The law of longitudinal change of morphology within inland branching channels as the ebb partition ratio and $D_{\geq 60,000}$ change is reflected in the

250 plan distributions of riverbed erosion/deposition rates during different periods (Supplementary Text/Figures S1-S8, based on the bed-elevation

251 point data in Supplementary Table SI).

252 Offshore depo-center movement, corresponding ebb partition ratios, and runoff intensities

253 Table II shows that changes in position of the offshore depo-center appear to follow a certain pattern according to variations in the multi-year

254 average ebb partition ratio of most inland branching channels of the bifurcations (except branching channels of the third and the fourth bifurcations

255 after the 2004-2007 and 2009-2011 periods, respectively) and $D_{\geq 60,000}$. In short, the offshore depo-center moved southward or southeastward, with

256 the multi-year average ebb partition ratios of the north/south branching channels of the bifurcations exhibiting general increase/decrease, as the

257 multi-year average value of $D_{\geq 60,000}$ rose. Conversely, the offshore depo-center moved northward, and the multi-year average ebb partition ratios of

258 the north/south branching channels of the bifurcations tended to decrease/increase, as the multi-year average value of $D_{\geq 60,000}$ reduced. The

259 critical value of $D_{\geq 60,000}$ between the southward/southeastward and northward movements was about 6 days yr^{-1}.

260 **Discussion**

261 Functional mechanism between morphology and hydrodynamics

262   A systematic linkage-mode can be identified (Figure 4) based on longitudinal morphological changes within the inland branching channels,

263 movement of the offshore depo-center, and corresponding variations in ebb partition ratio and $D_{\geq 60,000}$. The linkage-mode may be summarized as

264 follows. As $D_{\geq 60,000}$ increases, sediment in the inland north/south branching channels of the bifurcations tends to be transported

265 downstream/upstream, with deposition mainly occurring in the lower/upper sub-reaches (or more downstream/upstream channels), while the

266 offshore depo-center moves southward or southeastward. As $D_{\geq 60,000}$ lowers, sediment in inland north/south branching channels of the bifurcations

267 tends to deposit in the upper/lower sub-reaches (or more upstream/downstream channels), and the offshore depo-center moves northward.

268   Under varying runoff intensity, the linkage-mode is related to the pattern of horizontal circumfluence in the Yangtze Estuary and hydrodynamic

269 variations among the inland branching channels. In the Yangtze Estuary, the flood-tide discharge mainly flows northwestward from the offshore

270 area into the inland branching channels whereas the ebb-tide discharge usually flows southeastward from the inland branching channels into the

271   offshore area (Chen *et al.*, 1982; Li *et al.*, 2011). This promotes the formation of an anticlockwise horizontal circumfluence surrounding the whole

272   estuary and each bifurcation (Figure 5; Yan *et al.*, 2007; Shen & Li, 2011).

273   Changes in runoff discharge cause the flow pattern to vary among the inland branching channels, disturbing the horizontal circumfluence in

274   the Yangtze Estuary and altering the longitudinal morphological changes of channels and the position of the offshore depo-center. Figure 6

275   illustrates that the ebb partition ratios of the inland north/south branching channels of the bifurcations increase/decrease as runoff discharge grows,

276   and decrease/increase as runoff discharge lowers. This is related to the inertia of the ebb flow and the presence of northeastward raised nodes

277   along the south bank of the Yangtze Estuary (Zhu BY *et al.*, 2017). Given that the total ebb tidal discharge is stable at the yearly time scale,

278   more/less ebb tidal discharge is allocated to the north/south branching channels as runoff discharge grows. The opposite occurs as runoff

279   discharge reduces. Thus, as the value of $D_{\geq 60,000}$ increases, the horizontal circumfluence in the Yangtze Estuary becomes suppressed, and the

280   flow is compelled to shift from the anticlockwise- to the clockwise-direction (Shen & Li, 2011). Consequently, flood tides in the north/south

281   branching channels are relatively weakened/strengthened (Figure 4a), leading to downstream/upstream sediment transport in the north/south

282   branching channels, being carried by the ebb/flood tidal discharge (Figure 4a), resulting in increased deposition in the lower/upper sub-reaches (or

283   more downstream/upstream channels). Meanwhile, the northwestward flood tides in the offshore area are relatively weakened, resulting in

284   southward or southeastward movement of the offshore depo-center, driven by the ebb tidal current as it flows out of the mouths of the north

285   branching channels (Figure 4a). Conversely, as the value of $D_{\geq 60,000}$ lowers, an anticlockwise horizontal circumfluence in the Yangtze Estuary is

286   activated (Shen & Li, 2011). Consequently, the flood tides in the north branching channels strengthen as those in the south branching channels

287   weaken (Figure 4b), leading to upstream/downstream sediment transport in the north/south branching channels, driven by the flood/ebb tidal

288   discharge (Figure 4b), resulting in further deposition in the upper/lower sub-reaches (or more upstream/downstream channels). At the same time,

289   the northwestward flood tide strengthens in the offshore area, causing the offshore depo-center to move northward (Figure 4b).

290   Impact of estuarine engineering projects on regional channel morphology

291   The preceding analysis reveals that change in runoff discharge is the dominant factor influencing the overall pattern of longitudinal changes in

292   morphology within the inland branching channels and the movement of the offshore depo-center in the Yangtze Estuary. Nevertheless, the North

293   Branch and the South Passage witnessed outlier events (Table I; Supplementary Texts S1 and S8). In the North Branch, riverbed deposition rates

294   in the upper sub-reach exceeded those in the lower sub-reach during the flood periods of 1991-1998 and 1998-2001 (corresponding to high

295   values of $D_{\geq 60,000}$ of 26 days yr^{-1} and 36 days yr^{-1}). However, riverbed deposition rates in the upper sub-reach were smaller than those in the lower

296   sub-reach during the dry periods of 1978-1991 and 2001-2007 (with correspondingly low values of $D_{\geq 60,000}$ of 6 days yr^{-1} and 3 days yr^{-1}), indicating

297   downstream transport of sediment as $D_{\geq 60,000}$ decreased. This contradicts the supposed upstream transport of sediment, given that the North

298   Branch is the north branching channel of the first bifurcation. In the South Passage, both the upper and lower sub-reaches experienced erosion

299   during the flood-dominated period of 1997-2002 (when $D_{\geq 60,000}$ had a high value of 29 days yr^{-1}), implying that sediment was mainly deposited

300   offshore of the South Passage during this period. However, both sub-reaches underwent accretion during the dry period of 2002-2007 (associated

301   with a low value of $D_{\geq 60,000}$ of 4 days yr^{-1}). Meanwhile, the riverbed deposition rate in the upper sub-reach was smaller than in the lower sub-reach.

302   This suggests an upstream transport of sediment from the offshore area into the lower sub-reach of the South Passage as $D_{\geq 60,000}$ reduced, during

303   this period, contradicting the supposed downstream transport of sediment, noting that the South Passage is the south branching channel of the

304   fourth bifurcation. Land reclamation along the North Branch and the Deepwater Channel Project in the North Passage might be respectively

305 responsible for the outliers.

Impact of land reclamation along the North Branch

307 Land reclamation has caused the boundary of the North Branch to shrink (Figure 3). Table III shows that the reduction in channel volume of

308 the North Branch due to boundary change invariably exceeded 40% during the four periods considered, and even approached 90%, meaning that

309 the effect of boundary change was comparable to (or even more severe than) that of natural sediment deposition on morphological change of the

310 North Branch. During the last period, 2007-2013, the reduction in channel volume could be attributed to boundary change, given natural erosion in

311 the North Branch (Table III). During the periods considered before 2001, land reclamation was primarily implemented along the upper sub-reach

312 (Figure 3), promoting deposition in the upper sub-reach, especially during the flood period of 1998-2001 when the boundary change contribution

313 reached a remarkable value of 88% (Table I; Figure S1a-c; Table III). Given that the upper-reach was sheltered by land reclamation projects and

314 experienced heavy deposition, the flood river discharge during this period solely eroded the lower sub-reach (Table I; Figure S1c), leading to an

315 obvious increase in upstream sediment transport relative to the former two periods. On the contrary, after 2001, land reclamation implemented

316 along the lower sub-reach (Figure 3) caused sedimentation in the lower sub-reach during the dry period of 2001-2007 (Table I; Figure S1d),

317 resulting in downstream transport of sediment (relative to that in the flood period of 1998-2001). Land reclamation drove deposition/erosion in the

318 upper/lower sub-reach (Table I; Figure S1e) during the dry period of 2007-2013. And the constricted river boundary (Figure 3) helped strengthen

319 the flood tidal discharge in the North Branch (Dai *et al.*, 2016). Simultaneously, the low runoff discharge weakened the overall ebb tidal discharge

320 (Figure 6a), as confirmed by the negative value of ebb partition ratio for the North Branch and low value of $D_{\geq 60,000}$ during this period (Table I).

321 Hence, the flood tidal discharge scoured the lower sub-reach and carried eroded sediment into the upper sub-reach, causing deposition in the

322 upper sub-reach (Table I; Figure S1e).

323 Channel volume change rates between adjacent isobaths, located 1 m apart in the vertical direction (Figure 7) further reflect the influence of

324 land reclamation on morphological changes in the North Branch. Although the lower sub-reach underwent erosion during the flood period of

325 1998-2001 (Table I; Figure S1c), erosion mainly occurred in the deep area below the -4 m isobath, with deposition in the shallow area above the -4

326 m isobath (Figure 7) because of the sheltering effect of land reclaimed along the lower sub-reach before 2001 (Figure 3). A similar situation

327 occurred in the lower sub-reach during 1991-1998 (Figure 7), even though deposition occupied the whole of the lower sub-reach (Table I; Figure

328 S1b). During the other three periods of interest, the upper and lower sub-reaches generally experienced more deposition in shallow areas than

329 deep areas (Figure 7). The foregoing demonstrates the deposition-promotion effect of land reclamation, which interfered with the longitudinal

330 erosion-deposition pattern in the North Branch.

331 Within the whole North Branch, sediment underwent arbitrary longitudinal transport, reflected by the riverbed erosion/deposition rates in the

332 upper and lower sub-reaches (Table I). Longitudinal sediment transport within the lower sub-reach presented a better situation, indicated by the

333 riverbed erosion/deposition rates in the upper and lower segments of the lower sub-reach (Table IV). In the upper segment, deposition altered to

334 erosion from 1978-1991 and 1991-1998 (with low values of ebb partition ratio and $D_{\geq 60,000}$) to the flood period of 1998-2001 (with higher values of

335 ebb partition ratio and $D_{\geq 60,000}$); the rate of erosion became negative or declined in the upper segment during the latter dry periods of 2001-2007

336 and 2007-2013 (with lower values of ebb partition ratio and $D_{\geq 60,000}$) (Table IV). Moreover, the deposition/erosion rates in the upper segment were

337 larger/smaller than those in the lower segment during the dry periods of 2001-2007 and 2007-2013 (Table IV). These changes suggest that

338 sediment transport within the lower sub-reach tends to be directed downstream/upstream as the ebb partition ratio and runoff discharge

339 increase/decrease, unlike sediment transport within the whole North Branch. This confirms the disruption caused by land reclamation to

340 longitudinal sediment transport in the North Branch, given that the lower sub-reach experienced less total land reclamation than the upper

341 sub-reach (Figure 3).

342 **Impact of the Deepwater Channel Project**

343 Arbitrary longitudinal transport of sediment in the South Passage, evidenced by riverbed erosion/deposition rates in the two sub-reaches of

344 the South Passage (Table I), was influenced by spur-dike construction conducted as part of the Deepwater Channel Project.

345 The upper sub-reach experienced more severe erosion than the lower sub-reach of the South Passage during the flood period of 1997-2002

346 (with a lower value of ebb partition ratio and higher value of $D_{\geq 60,000}$) (Table I) owing to the first stage of spur-dike construction along the upper

347 sub-reach of the North Passage during this period (Dai *et al.*, 2013). The spur dikes hindered the ebb tidal current in the North Passage while

348 intensifying the strength of the ebb tide in the South Passage, exacerbating erosion in the upper sub-reach of the South Passage (Table I). Erosion

349 of both the upper and lower sub-reaches of the South Passage mainly occurred in the deeper regions during this period (Figure 8), indicating an

350 obvious effect of water retention in the deep channel (Li *et al.*, 2018) of the South Passage due to the strengthened ebb tide in the South Passage.

351 The greater severity of deposition in the lower sub-reach than in the upper sub-reach in the South Passage (associated with a higher value of

352 ebb partition ratio and lower value of $D_{\geq 60,000}$) during the dry period of 2002-2007 (Table I) was also partly related to water retention in the deep

353 channel of the South Passage. Spur dikes had been constructed along both upper and lower sub-reaches of the North Passage during this period

354 (Dai *et al.*, 2013), causing the blockage effect of the North Passage on the ebb tidal current to become enhanced, and the ebb tide in the South

355 Passage strengthen, as evidenced by the decrease/increase in ebb partition ratio in the North/South Passage (Table I). This in turn promoted a

stronger ebb tidal current in the deep area of the South Passage due to water retention in the deep channel (Li *et al.*, 2018), eroding the thalweg of the upper sub-reach and transporting eroded sediment into the thalweg of the lower sub-reach of the South Passage (Figure 8), causing remarkable deposition to occur in the lower sub-reach (Table I).

Apart from their impact on longitudinal morphological change, the estuarine engineering projects also affected the flow dynamics within certain channels. The ebb partition ratio of the North Channel presented an almost monotonic increasing trend after 2004-2007, rather than correlating with the growth and reduction in runoff discharge during former periods (Table II). This occurred because construction of the Qingcaosha Reservoir from 2007 to 2011 near the head of the North Channel narrowed the channel entrance (Figure 1b) and strengthened the ebb tidal current in the channel (Mei *et al.*, 2018). Correspondingly, the ebb partition ratio of the South Channel presented a monotonic decreasing trend after 2004-2007 (Table II). The ebb partition ratio of the North Passage exhibited an overall decrease after 2009-2011, again unlike the correlation with runoff discharge in former periods (Table II). This was caused by construction of spur dikes as part of the Deepwater Channel Project completed in 2010 (Dai *et al.*, 2013), which obstructed the North Passage (Figure 1b) and weakened its ebb tidal current field. Accordingly, the ebb partition ratio of the South Passage showed an overall increase after 2009-2011 (Table II).

Progress in channel longitudinal evolution and offshore depo-center movement

Historical courses

Since the 1950s, more than 50,000 dams have been built in the Yangtze River basin, which have flattened the intra-annual distribution of runoff discharge (especially the large cascade dams constructed in the upper Yangtze, Figure 1a) (Yang *et al.*, 2011; Zhu BY *et al.*, 2017). Under the runoff flattening effect, multi-year average duration days of high-level discharges (> 50,000 m^3 s^{-1}) and low-level discharges (< 10,000 m^3 s^{-1})

373 have decreased remarkably, those of middle-low-level discharges (10,000-20,000 m^3 s^{-1}) have increased significantly, and those of

374 middle-high-level discharges (20,000-50,000 m^3 s^{-1}) have changed little (Figure 9).

375   By considering the relationships between ebb partition ratios of the inland branching channels and runoff discharge (Figure 6), the ebb

376 partition ratios of the north/south branching channels experienced decreasing/increasing trends as runoff discharge flattening occurred (Figure 10).

377 Based on the functional mechanism connecting longitudinal changes of morphology within inland branching channels, movement of offshore

378 depo-center, ebb partition ratios, and runoff intensity, the major depositional areas in the north/south branching channels generally underwent

379 overall migration upstream/downstream, except for those channels impacted by estuarine engineering projects (Figure 11); simultaneously, the

380 offshore depo-center migrated northward (Table II). This is now discussed in detail.

381   Ebb partition ratios for the North and South Branches at the first bifurcation experienced decreasing and increasing trends (Figure 10a).

382 Sediment in the South Branch was transported downstream, with greater increases in net erosion rate in upper sub-reaches D and E than in lower

383 sub-reach F (Figure 11a). However, sediment in the North Branch was transported upstream before 2003, after which it moved downstream.

384 Before 2003, the ratio of channel volume below the 0 m isobath of the upper sub-reach A and middle sub-reach B to the total volume below the 0

385 m isobath of the North Branch underwent a declining trend, while the ratio of the lower sub-reach C increased. After 2003, an overall reversal

386 occurred in the trends in ratios of the sub-reaches (Figure 11a). This reversal was mainly caused by land reclamation along the upper sub-reach of

387 the North Branch before 2001 and the lower sub-reach after 2001 (Figure 3), which accordingly promoted deposition in each of the sub-reaches.

388   Ebb partition ratios of the North and South Waterways of Baimao Shoal at the second bifurcation experienced decreasing and increasing

389 trends (Figure 10b). The major depositional area in the North/South Waterway moved upstream/downstream, accompanied by

390 decreasing/increasing trends in the ratio of channel volume below 0 m isobath of the upper/lower sub-reaches to the total channel volume below 0

391 m isobath of the North Waterway, and increasing/decreasing trends in the ratio for the two sub-reaches of the South Waterway (Figure 11b).

392 For the North/South Channel at the third bifurcation, the temporal variation in ebb partition ratio could be divided (roughly) into two stages.

393 Before 1988, the ebb partition ratio of the North/South Channel decreased/increased (Figure 10c), due to dam-induced runoff flattening. After

394 1988, the ebb partition ratios of the two branching channels respectively increased and decreased (Figure 10c), due to extreme floods in 1998 and

395 1999 (Zhu BY et al., 2017) and impoundment of the Qingcaosha Reservoir. As a result, the major depositional area in the North Channel altered its

396 direction of migration from upstream before 1986 to downstream after 1986, with the average water depth decreasing at cross-section 1-1' and

397 increasing at cross-sections 2-2' and 3-3' before 1986, and the reverse (approximately) occurring after 1986 (Figure 11c). In the South Channel,

398 sediment was transported upstream from the watercourse downstream of the South Channel to the lower sub-reach of the South Channel. This

399 caused erosion in both sub-reaches of the South Channel before 2006, and deposition in the two sub-reaches (with more deposition in the lower

400 sub-reach) after 2006 (Figure 11c).

401 For the North/South Passage at the fourth bifurcation, the variation in ebb partition ratio also appears to have experienced two phases. Before

402 1999, the ebb partition ratio of the North/South Passage increased/decreased (Figure 10d) because the North Passage underwent forming

403 development during this stage (Yun, 2004; Zhu BY et al., 2017). After 1999, the ebb partition ratios of the two branching channels respectively

404 decreased and increased (Figure 10d), due to implementation of the Deepwater Channel Project and the flattening effect on runoff discharge

405 caused by the Three Gorges Dam (TGD) and other large cascade dams (e.g. XLDD and XJD) in the upper Yangtze (Figure 1a; Figure 9). The

406 major depositional area in the North Passage moved upstream after 2000, with the distance reducing between the sedimentary body and

Hengsha station (Figure 1b), especially after 2004 (Figure 11d). Meanwhile, the major depositional area in the South Passage moved downstream after 2002, with the mean water depth increasing at cross-sections 4-4' and 5-5' after 2007 and decreasing at cross-section 6-6' after 2002 (Figure 11d).

Noting the overall decreasing/increasing trends in ebb partition ratios of the inland north/south branching channels, the offshore depo-center has migrated northward in recent years, particularly after 2003 when the Three Gorges Dam (TGD) and other large cascade dams (e.g. XLDD and XJD) began to impound water, except during the flood period of 2009-2011 (Table II).

Future trends

At the time of writing, a cascade of large dams is being constructed along the upper Yangtze. These dams will result in a continuous flattening effect on runoff discharge in the future (Duan *et al.*, 2016) with ongoing overall decreases/increases in ebb partition ratios of the inland north/south branching channels. Now that several major estuarine engineering projects, including land reclamation along the North Branch, the Deepwater Channel Project in the North Passage and the Qingcaosha Reservoir in the North Channel, have been completed (Dai *et al.*, 2013, 2016; Mei *et al.*, 2018), their impact on ebb partition ratios of the inland branching channels will persist. Therefore, recent trends in longitudinal changes of morphology within the inland branching channels and movement of depo-center in the offshore area are likely to continue into the future, provided the Yangtze Estuary experiences no new significant human interference.

Conclusions

The present study shows that major depositional areas within the inland north branching channels of the Yangtze estuarine bifurcations moved downstream/upstream as the multi-year average ebb partition ratios and $D_{\geq 60,000}$ increased/decreased. Movements of major depositional

424 areas within the inland south branching channels exhibited opposing behavior. The Yangtze offshore depo-center moved southward (or

425 southeastward) or northward as the ebb partition ratios and $D_{\geq 60,000}$ rose or declined. The critical value of $D_{\geq 60,000}$ separating southward (or

426 southeastward) and northward movements of the offshore depo-center was about 6 days yr^{-1}. The mechanism behind this decadal linkage-mode

427 of inland longitudinal morphological evolution and offshore depo-center movement in the Yangtze Estuary is related to variations in ebb partition

428 ratios of the inland north/south branching channels under varying runoff discharge. Under rising runoff discharge, the ebb partition ratios of the

429 inland north/south branching channels increase/decrease, causing the horizontal circumfluence in the Yangtze Estuary to shift rotational direction

430 from anticlockwise to clockwise. Sediment within the inland north/south branching channels is then forced downstream/upstream, and the offshore

431 depo-center pushed southward (or southeastward). Under declining runoff discharge, the opposite situation prevails.

432 Longitudinal erosion-deposition patterns in the North Branch and South Passage during all periods of interest, and variations in ebb partition

433 ratios of the North/South Channel since 2004-2007 and the North/South Passage since 2009-2011, were disrupted by estuarine engineering

434 projects. The position of the major depositional area in the North Branch almost kept pace with the location of land reclamation works when the

435 contributing proportion from land reclamation was between 41% and 136%. The position of the major depositional area in the South Passage was

436 affected by the construction of spur-dikes as part of the Deepwater Channel Project in the North Passage. These dikes blocked the North Passage

437 and intensified the ebb tide in the South Passage. This led to erosion in the deep area of the upper sub-reach of the South Passage caused by

438 water retention in the deep channel, and deposition or reduced erosion in the lower sub-reach of the South Passage of sediment sourced from the

439 upper sub-reach carried by the ebb tidal current. Outlier ebb partition ratio variations in the North/South Channel and the North/South Passage

440 were triggered by the strengthening effect on the ebb tide of the Qingcaosha Reservoir (constructed near the head of the North Channel) and the

441 weakening effect on the ebb tide of spur dikes (of the Deepwater Channel Project) built in the North Passage.

442 Owing to runoff flattening caused by river dams, the major depositional areas within the inland north/south branching channels and the

443 depo-center in the offshore area of the Yangtze Estuary generally experienced historical trajectories of upstream, downstream, and northward

444 movements, respectively, except in those areas impacted by estuarine engineering projects. With the continuing construction of large cascade

445 dams along the upper Yangtze and the completion of major estuarine engineering projects, it is likely that the dam-induced historical trends in

446 longitudinal morphological evolution of the inland branching channels and movement of the offshore depo-center are likely to continue into the

447 future.

References

449 Baek YS, Lee SH, Chang TS. 2017. Last interglacial to Holocene sedimentation on intertidal to subtidal flats revealed by seismic and deep-core sediment analyses,

450 southwest coast of Korea. *Quaternary International* **459**: 45-54. https://doi.org/10.1016/j.quaint.2017.08.001

451 Cai H, Savenije HHG, Toffolon M. 2014. Linking the river to the estuary: influence of river discharge on tidal damping. *Hydrology and Earth System Sciences* **18**(1):

452 287-304. https://doi.org/10.5194/hess-18-287-2014

453 Changjiang Water Resources Commission (CWRC). 2017. *Changjiang River Sediment Bulletin*. Changjiang Press: Wuhan, China, 4-7. URL:

454 http://www.cjw.gov.cn/zwzc/bmgb/

455 Chen J, Li D. 2002. *Regulation of the Changjiang Estuary: Past, Present and Future*. Springer: Berlin, Germany, 185-197.

456 Chen JY, Yun CX, Xu HG. 1982. The Model of Development of the Changjiang Estuary during the last 2000 years. In *Estuarine Comparisons*, Kennedy VS (ed).

457 Academic Press: State of Utah, America, 655-666. https://doi.org/10.1016/B978-0-12-404070-0.50047-8

458 Dai ZJ, Fagherazzi S, Mei XF, Chen JY, Meng Y. 2016. Linking the infilling of the North Branch in the Changjiang (Yangtze) estuary to anthropogenic activities from

459 1958 to 2013. *Marine Geology* **379**: 1-12. https://doi.org/10.1016/j.margeo.2016.05.006

460 Dai ZJ, Liu JT, Fu G, Xie HL. 2013. A thirteen-year record of bathymetric changes in the North Passage, Changjiang (Yangtze) estuary. *Geomorphology* **187**(4):

461 101-107. https://doi.org/10.1016/j.geomorph.2013.01.004

462 Dai ZJ, Liu JT, Wei W, Chen JY. 2014. Detection of the Three Gorges Dam influence on the Changjiang (Yangtze River) submerged delta. *Scientific Reports* **4**: 6600.

463 https://doi.org/10.1038/srep06600

464 Dou GR. 1964. The bed form of the alluvial streams and the tidal delta. *SHUILI XUEBAO* (2): 1-13. https://doi.org/10.13243/j.cnki.slxb.1964.02.001 (in Chinese)

465 Du JL, Yang SL, Feng H. 2016. Recent human impacts on the morphological evolution of the Yangtze River delta foreland: A review and new perspectives. *Estuarine*

466 *Coastal and Shelf Science* **181**: 160-169. https://doi.org/10.1016/j.ecss.2016.08.025

467 Duan WX, Guo SL, Wang J, Liu DD. 2016. Impact of cascaded reservoirs group on flow regime in the middle and lower reaches of the Yangtze River. *Water* **8**(6): 1-21.

468 https://doi.org/10.3390/w8060218

469 El Jakani M, Ettazarini S, Rhinane H, Raji M, Radid M, Talbi M. 2019. Impact of anthropogenic facilities on the morphodynamic evolution of an estuarine system: the

470 case of Oum Er-Rbia Estuary (Azemmour, Morocco). *Journal of Marine Science and Engineering* **7**(8): 248. https://doi.org/10.3390/jmse7080248

471 Fletcher CH, Knebel HJ, Kraft JC. 1992. Holocene depocenter migration and sediment accumulation in Delaware Bay: A submerging marginal marine sedimentary

472 basin. *Marine Geology* **103**(1-3): 165-183. https://doi.org/10.1016/0025-3227(92)90014-9

473 Frihy O, Lawrence D. 2004. Evolution of the modern Nile delta promontories: development of accretional features during shoreline retreat. *Environmental Geology*

474 **46**(6-7): 914-931. https://doi.org/10.1007/s00254-004-1103-3

475   Gu JL, Luo M, Zhang XJ, Christakos G, Agusti S, Duarte CM, Wu JP. 2018. Losses of salt marsh in China: Trends, threats and management. *Estuarine Coastal and*

476   *Shelf Science* **214**: 98-109. https://doi.org/ 10.1016/j.ecss.2018.09.015

477   Han JQ, Huang LB. 2018. Numerical experiments on stagnation points influenced by the Three Gorges Dam in the Yangtze Estuary. *Water Science and Technology –*

478   *Water Supply* **18**(3): 1032-1040. https://doi.org/ 1032-1040

479   Hanebuth TJJ, Lantzsch H, Nizou J. 2015. Mud depocenters on continental shelves-appearance, initiation times, and growth dynamics. *Geo-Marine Letters* **35**(6):

480   487-503. https://doi.org/10.1007/s00367-015-0422-6

481   Jiang CJ, Li JF, de Swart HE. 2012. Effects of navigational works on morphological changes in the bar area of the Yangtze Estuary. *Geomorphology* **139**: 205-219.

482   https://doi.org/10.1016/j.geomorph.2011.10.020

483   Lee SH, Kim MJ, Kim CS, Choi BJ, Moon HB. 2017. Surface circulation and vertical structure of current off the Keum River Estuary, Korea in later spring 2008. *Ocean*

484   *Science Journal* **52**(3): 307-327. https://doi.org/10.1007/s12601-017-0043-2

485   Li L, Zhu JR, Wu H, Wang B. 2010. A numerical study on water diversion ratio of the Changjiang (Yangtze) estuary in dry season. *Chinese Journal of Oceanology and*

486   *Limnology* **28**(3): 700-712. https://doi.org/ 10.1007/s00343-010-9114-2

487   Li MT, Chen ZY, Yin DW, Chen J, Wang ZH, Sun QL. 2011. Morphodynamic characteristics of the dextral diversion of the Yangtze River mouth, China: tidal and the

488   Coriolis Force controls. *Earth Surface Processes and Landforms* **36**(5): 641-650. https://doi.org/10.1002/esp.2082

489   Li SX, Li YT, Yuan J, Zhang W, Chai YF, Ren JQ. 2018. The impacts of the Three Gorges Dam upon dynamic adjustment mode alterations in the Jingjiang reach of the

490   Yangtze River, China. *Geomorphology* **318**: 230-239. https://doi.org/10.1016/j.geomorph.2018.06.020

491   Liu H, He Q, Wang ZB, Weltje GJ, Zhang J. 2010. Dynamics and spatial variability of near-bottom sediment exchange in the Yangtze Estuary, China. *Estuarine Coastal*

492   *and Shelf Science* **86**(3): 322-330. https://doi.org/10.1016/j.ecss.2009.04.020

493   Liu J, Xu ZY, Zhao DZ, Cheng HF. 2009. Change of re-siltation in the Yangtze Estuary deepwater channel during 1st and 2nd stages. *Journal of Sediment Research* (2):

494   22-28. https://doi.org/10.16239/j.cnki.0468-155x.2009.02.008 (in Chinese)

495   Luan HL, Ding PX, Wang ZB, Ge JZ, Yang SL. 2016. Decadal morphological evolution of the Yangtze Estuary in response to river input changes and estuarine

496   engineering projects. *Geomorphology* **265**: 12-23. https://doi.org/10.1016/j.geomorph.2016.04.022

497   Maloney JM, Bentley SJ, Xe KH, Obelcz J, Georgiou IY, Miner MD. 2018. Mississippi River subaqueous delta is entering a stage of retrogradation. *Marine Geology* **400**:

498   12-23. https://doi.org/ 10.1016/j.margeo.2018.03.001

499   Marriner N, Flaux C, Morhange C, Stanley JD. 2013. Tracking Nile Delta vulnerability to Holocene change. *Plos One* **8**(7): e69195.

500   https://doi.org/10.1371/journal.pone.0069195

501   Mei XF, Dai ZJ, Wei W, Li WH, Wang J, Sheng H. 2018. Secular bathymetric variations of the North Channel in the Changjiang (Yangtze) Estuary, China, 1880-2013:

502   Causes and effects. *Geomorphology* **303**: 30-40. https://doi.org/10.1016/j.geomorph.2017.11.014

503   Nitsche FO, Ryan WBF, Carbotte SM, Bell RE, Slagle A, Bertinado C, Flood R, Kenna T, McHugh C. 2007. Regional patterns and local variations of sediment

504   distribution in the Hudson River Estuary. *Estuarine Coastal and Shelf Science* **71**(1-2): 259-277. https://doi.org/10.1016/j.ecss.2006.07.021

505   Nizou J, Hanebuth TJJ, Heslop D, Schwenk T, Palamenghi L, Stuut JB, Henrich R. 2010. The Senegal River mud belt: A high-resolution archive of paleoclimatic

506   change and coastal evolution. *Marine Geology* **278**(1-4): 150-164. https://doi.org/10.1016/j.margeo.2010.10.002

507   Ou HS, Wei CH, Deng Y, Gao NY. 2013. Principal component analysis to assess the composition and fate of impurities in a large river-embedded reservoir:

508   Qingcaosha Reservoir. *Environmental Science – Processes & Impacts* **15**(8): 1613-1621. https://doi.org/10.1039/c3em00154g

509   Rao KN, Subraelu P, Kumar KCVN, Demudu G, Malini BH, Rajawat AS, Ajai. 2010. Impacts of sediment retention by dams on delta shoreline recession: evidences

510   from the Krishna and Godavari deltas, India. *Earth Surface Processes and Landforms* **35**(7): 817-827. https://doi.org/ 10.1002/esp.1977

511   Robert A. 2017. A river in Peril: Human activities and environmental impacts on the lower Mekong River and its delta. *Environment* **59**(6): 30-40.

512   https://doi.org/10.1080/00139157.2017.1374794

513   Shen HT, Li JF. 2011. *Water and Sediment Transport in the Changjiang Estuary*. China Ocean Press: Beijing, China, 53-62, 69-75, 82-93, 170-180. (in Chinese)

514   Siverd CG, Hagen SC, Bilskie MV, Braud DH, Peele RH, Twilley RR. 2018. Hydrodynamic storm surge model simplification via application of land to water isopleths in

515   coastal Louisiana. *Coastal Engineering* **137**: 28-42. https://doi.org/10.1016/j.coastaleng.2018.03.006

516   Stanley DJ, Warne AG. 1993. Nile Delta: Recent geological evolution and human impact. *Science* **260**(5108): 628-634. https://doi.org/ 10.1126/science.260.5108.628

517   Wang YH, Ridd PV, Wu HL, Wu JX, Shen HT. 2008. Long-term morphodynamic evolution and the equilibrium mechanism of a flood channel in the Yangtze Estuary

518   (China). *Geomorphology* **99**(1-4): 130-138. https://doi.org/10.1016/j.geomorph.2007.10.003

519   Wei W, Tang ZH, Dai ZJ, Lin YF, Ge ZP, Gao JJ. 2015. Variations in tidal flats of the Changjiang (Yangtze) estuary during 1950s-2010s: Future crisis and policy

520   implication. *Ocean & Coastal Management* **108**: 89-96. https://doi.org/10.1016/j.ocecoaman.2014.05.018

521   Xu TY, Shi XF, Wang GQ, Qiao SQ, Yang G, Liu SF, Wang XC, Zhao QH. 2013. Sedimentary facies of the subaqueous Changjiang River delta since the late

522   Pleistocene. *Chinese Journal of Oceanology and Limnology* **31**(5): 1107-1119. https://doi.org/10.1007/s00343-013-2281-1

523   Yan YX, Tao AF, Yu DS, Yang JY. 2007. Analysis on the circulation of the Yangtze river estuary based on ADCP measurements. *China Ocean Engineering* **21**(3):

524   485-494. https://doi.org/10.1677/joe.0.0100046

525   Yang SL, Milliman JD, Li P, Xu K. 2011. 50,000 dams later: Erosion of the Yangtze River and its delta. *Global and Planetary Change* **75**(1-2): 14-20.

526 https://doi.org/10.1016/j.gloplacha.2010.09.006

527 Yang SL, Xu KH, Milliman, JD, Yang HF, Wu CS. 2015. Decline of Yangtze River water and sediment discharge: Impact from natural and anthropogenic changes.

528 *Scientific Reports* **5**: 12581. https://doi.org/10.1038/srep12581.

529 Yang YP, Zhang MJ, Li YT, Fan YY. 2016. Trend and dynamic cause of sediment particle size on the adjacent continental shelf of the Yangtze Estuary. *China Ocean*

530 *Engineering* **30**(6): 992-1003. https://doi.org/10.1007/s13344-016-0065-z

531 Yankovsky AE, Hickey BM, Munchow AK. 2001. Impact of variable inflow on the dynamics of a coastal buoyant plume. *Journal of Geophysical Research – Oceans*

532 **106**(C9): 19809-19824. https://doi.org/10.1029/2001JC000792

533 Yun CX. 2004. *Recent Developments of the Changjiang Estuary*. China Ocean Press: Beijing, China, 1-47. (in Chinese)

534 Zamora HA, Nelson SM, Flessa KW, Nomura R. 2013. Post-dam sediment dynamics and processes in the Colorado River estuary: Implications for habitat restoration.

535 *Ecological Engineering* **59**: 134-143. https://doi.org/10.1016/j.ecoleng.2012.11.012

536 Zhang M, Townend I, Zhou YX, Cai HY. 2016. Seasonal variation of river and tide energy in the Yangtze estuary, China. *Earth Surface Processes and Landforms* **41**(1):

537 98-116. https://doi.org/10.1002/esp.3790

538 Zhang WY, Gong Z, Zhang CK, Tan W. 2016. Response of nearshore circulation outside Yangtze Estuary to El Nino events. *Water Science and Engineering* **9**(2):

539 145-154. https://doi.org/10.1016/j.wse.2016.02.004

540 Zhao J, Guo LC, He Q, Wang ZB, van Maren DS, Wang XY. 2018. An analysis on half century morphological changes in the Changjiang Estuary: Spatial variability

541 under natural processes and human intervention. *Journal of Marine Systems* **181**: 25-36. https://doi.org/10.1016/j.jmarsys.2018.01.007

542 Zhou YY, Huang HQ, Ran LS, Shi CX, Su T. 2018. Hydrological controls on the evolution of the Yellow River Delta: An evaluation of the relationship since the

543   Xiaolangdi Reservoir became fully operational. *Hydrological Processes* **32**(24): 3633-3649. https://doi.org/10.1002/hyp.13274

544   Zhu BY, Li YT, Yue Y, Yang YP. 2017. Aggravation of north channels' shrinkage and south channels' development in the Yangtze Estuary under dam-induced runoff

545   discharge flattening. *Estuarine Coastal and Shelf Science* **187**: 178-192. https://doi.org/10.1016/j.ecss.2016.10.048

546   Zhu BY, Li YT, Yue Y, Yang YP, Liang EH, Zhang CC, Borthwick AGL. 2020. Alternate erosion and deposition in the Yangtze Estuary and the future change. *Journal of*

547   *Geographical Sciences* **30**(1): 145-163. https://doi.org/10.1007/s11442-020-1720-0

548   Zhu CY, Guo LC, van Maren DS, Tian B, Wang XY, He Q, Wang ZB. 2019. Decadal morphological evolution of the mouth zone of the Yangtze Estuary in response to

549   human interventions. *Earth Surface Processes and Landforms* **44**(12): 2319-2332. https://doi.org/10.1002/esp.4647

550

Acknowledgements

Data Availability Statement

The data sets used and/or analyzed during the current study are available from the corresponding author on reasonable request.

561
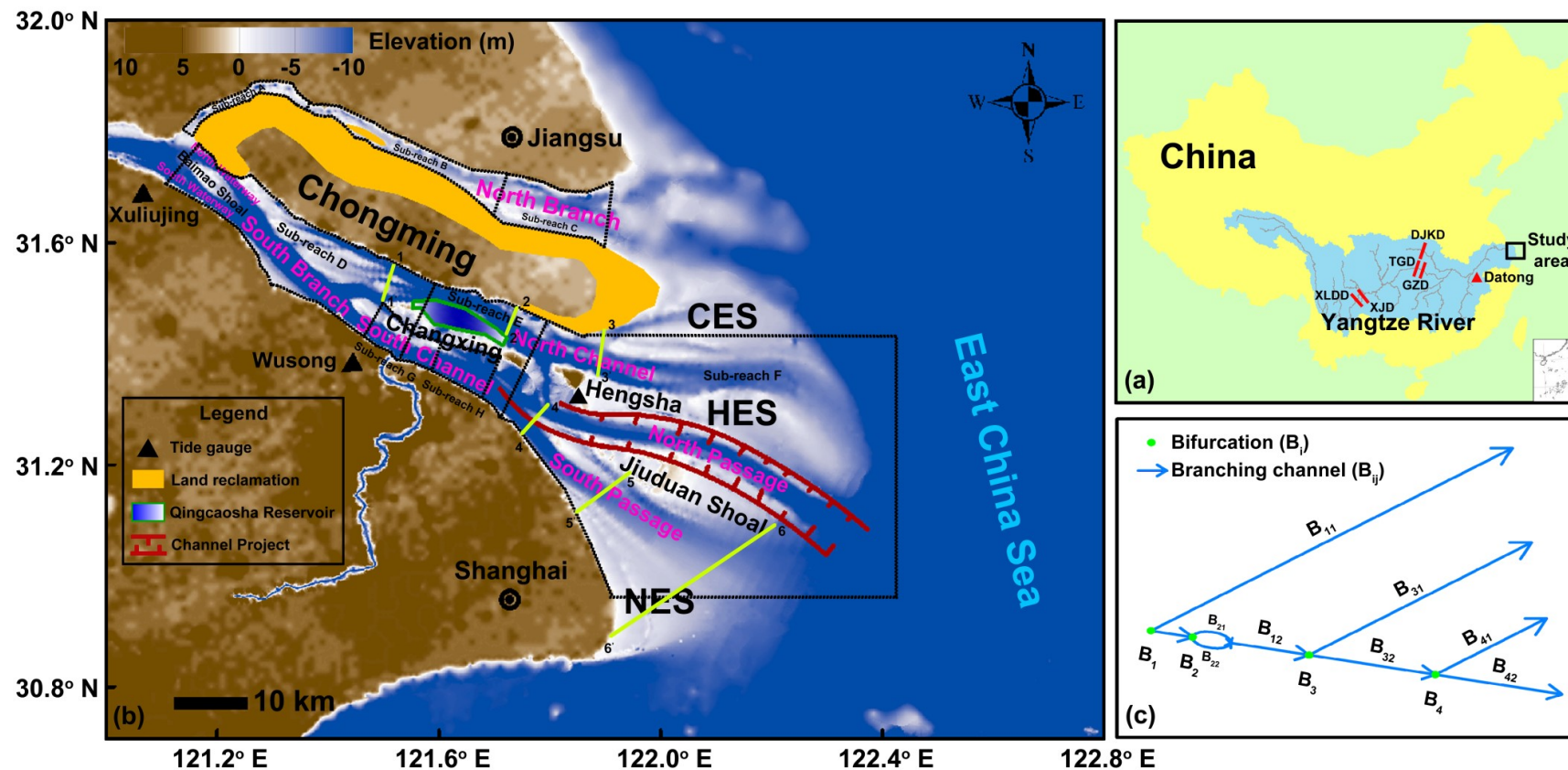
Figure 1. Plan view of the study area indicating key locations. (a) Locations of Datong station, Three Gorges Dam (TGD), Xiluodu Dam (XLDD), Xiangjia Dam (XJD), Gezhou Dam (GZD), and Danjiangkou Dam (DJKD) within the Yangtze River Basin, and the Yangtze Estuary (the study area). (b) Plan view of the Yangtze Estuary, showing the layouts of major engineering projects (land reclamation, Qingcaosha Reservoir, and Deepwater Channel Project); CES, HES, and NES represent Chongming East Shoal, Hengsha East Shoal, and Nanhui East Shoal; the sub-reaches (A, B, C, D, E, F, G, H) and cross-sections (1-1', 2-2', 3-3', 4-4', 5-5', 6-6') are the same as in Supplementary Table SI. (c) Sketch map showing the four orders of bifurcations. B_i indicates the i-th bifurcation (i = 1-4), and B_{ij} represents the j-th branch at B_i (j = 1-2).
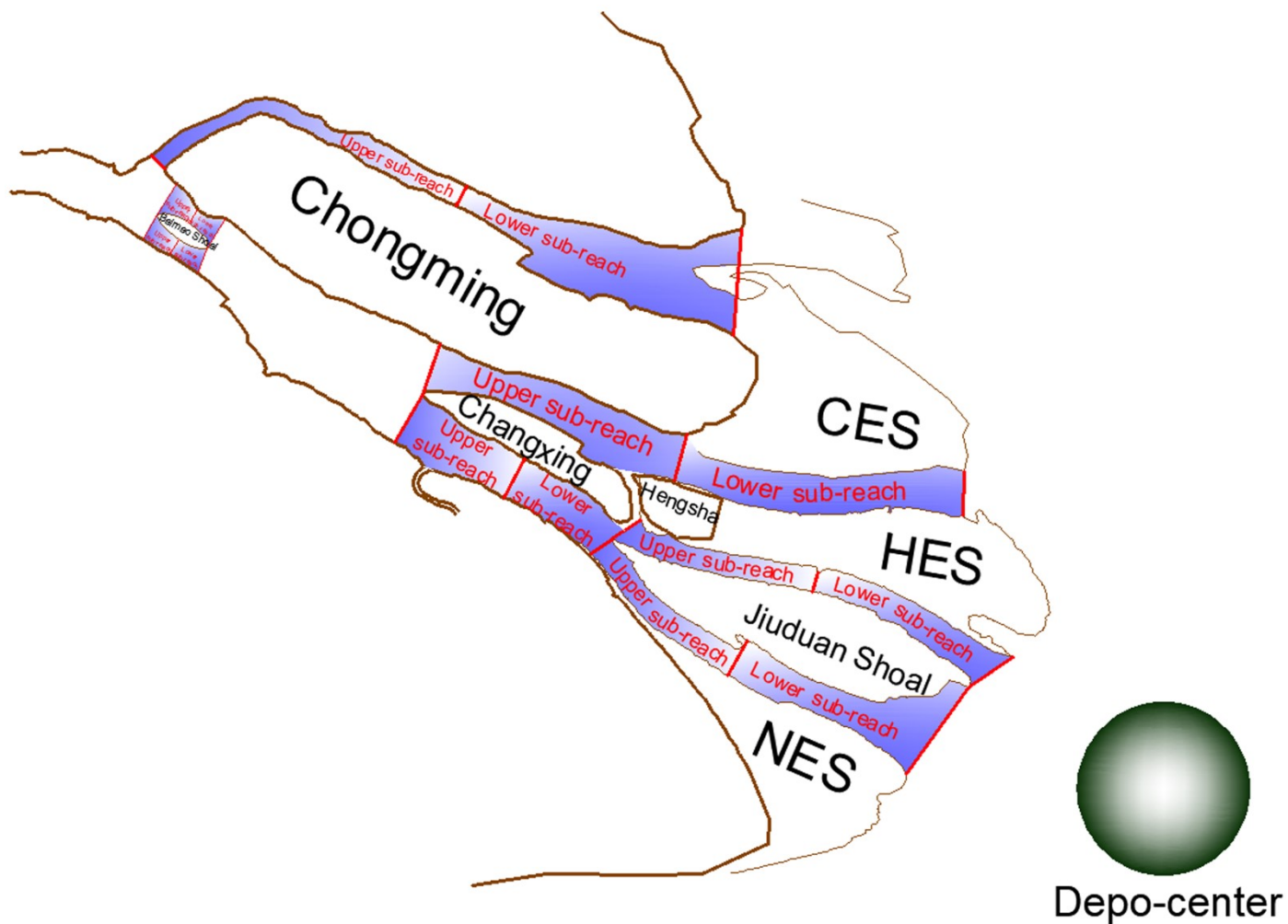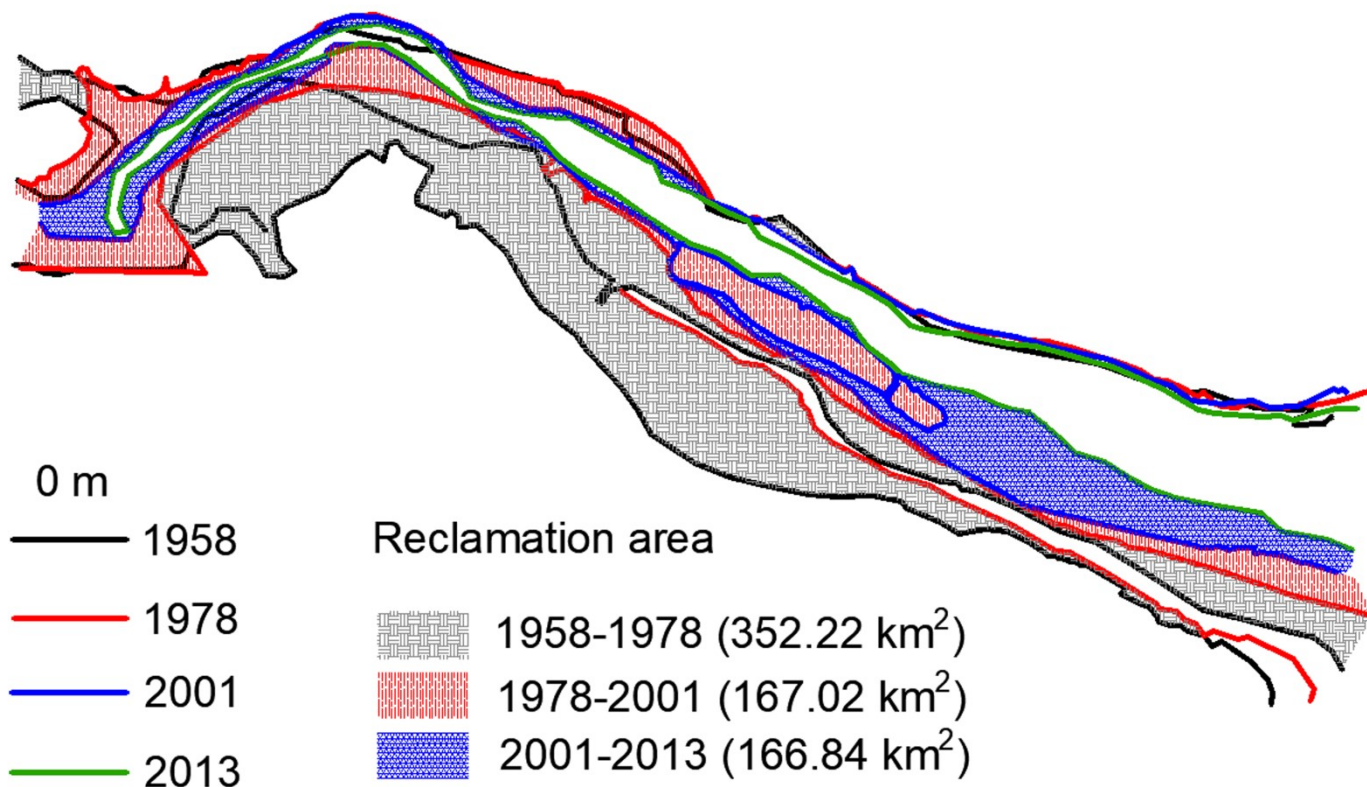
569

570

571 **Figure 2.** Sketch of sub-reach division of branching channels and offshore depo-center in the Yangtze Estuary.

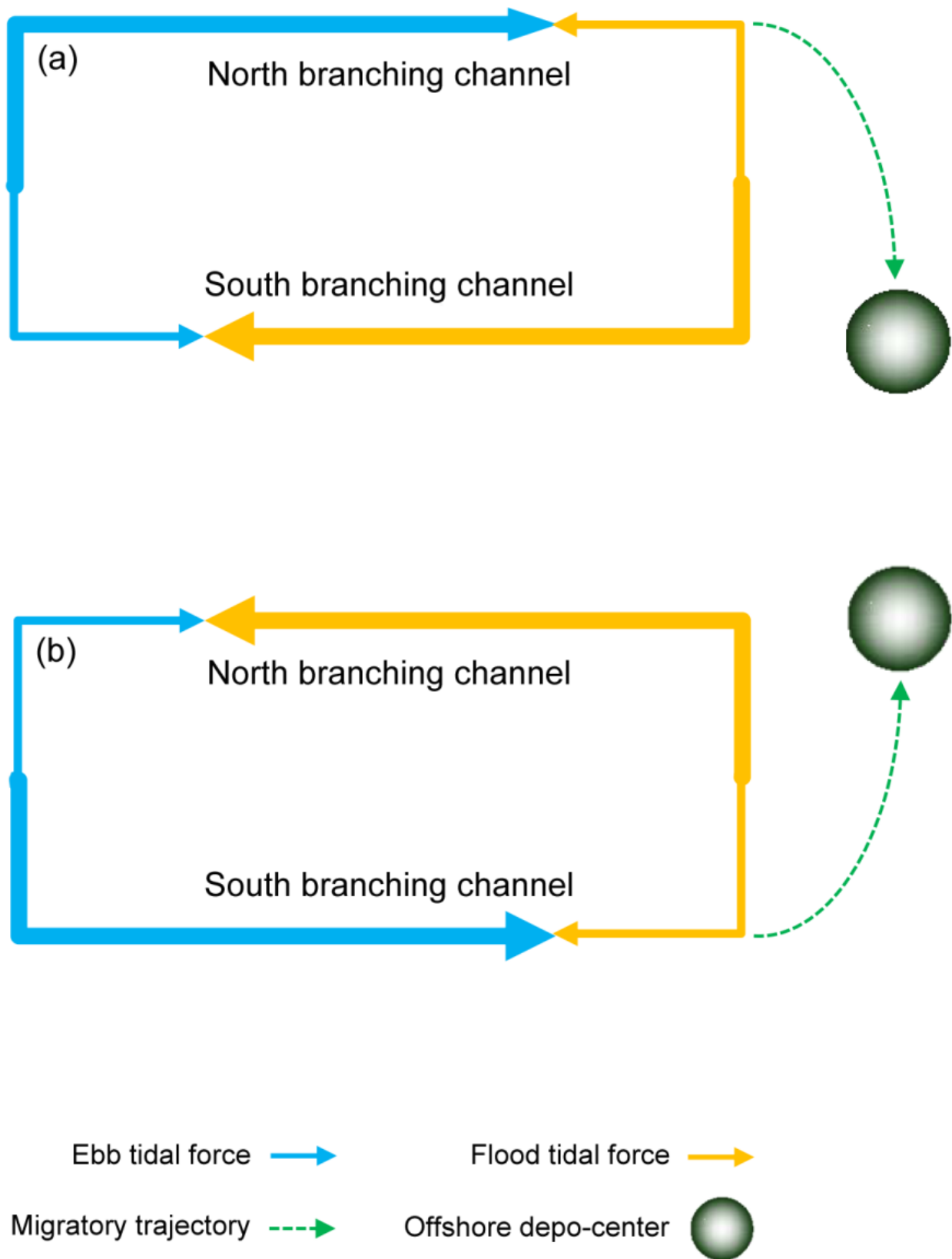572 The upper and lower sub-reaches of each branching channel are roughly the same length.

573

0 m

— 1958
— 1978
— 2001
— 2013

Reclamation area

1958-1978 (352.22 km^2)
1978-2001 (167.02 km^2)
2001-2013 (166.84 km^2)

574

575

576   **Figure 3.** Land reclamation along the North Branch from 1958 to 2013. Data provided by East China Normal

577   University (see Supplementary Table SI).

578

579

Figure 4. Sketch of variations in ebb and flood tidal forces in branching channels of given bifurcations and corresponding movement of the offshore depo-center in the Yangtze Estuary during periods that witness growth in $D_{\geq 60,000}$ (a) and reduction in $D_{\geq 60,000}$ (b). The length and thickness of the blue and orange arrows represent the strengths of the ebb and flood tidal forces.

Labels within figure: Chongming, Changxing, Hengsha, CES, HES, Jiuduan Shoal, NES, Biam'an Shoal
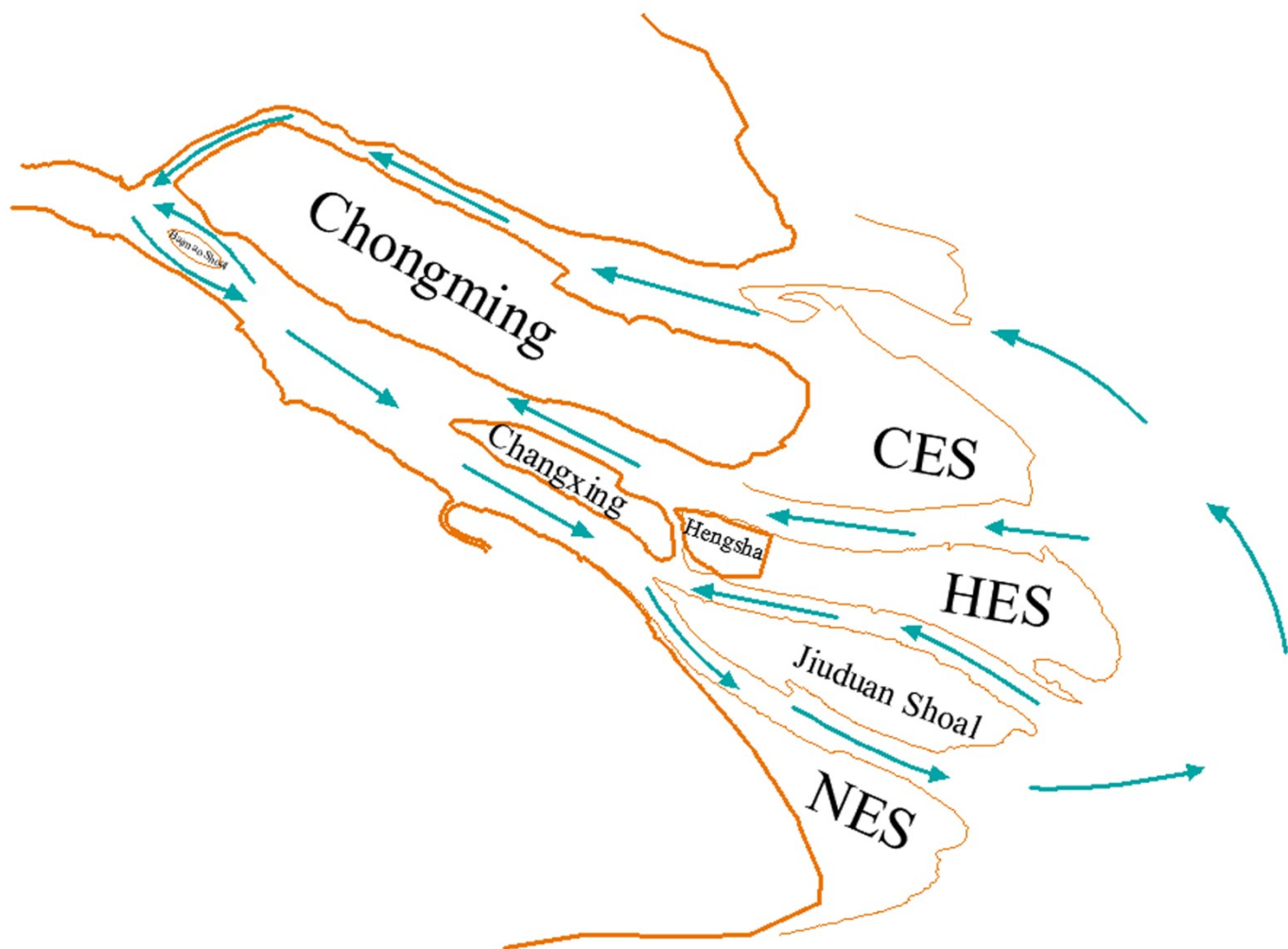
585

586

587 **Figure 5.** Sketch of horizontal circumfluence pattern in the Yangtze Estuary.
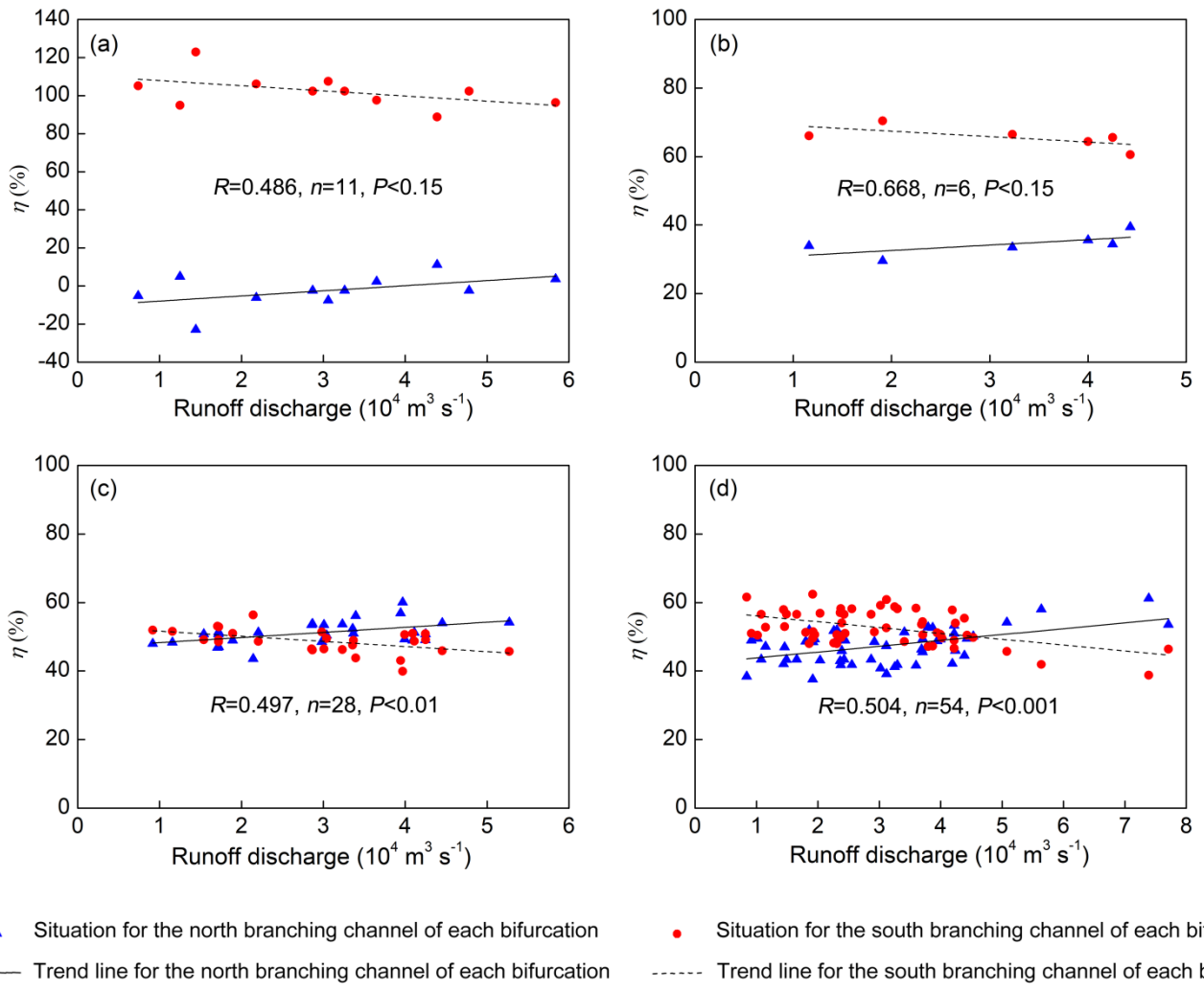
588

Figure 6. Variation in ebb partition ratio (η) with runoff discharge for branching channels of the Yangtze Estuary: (a) North/South Branch (Dai *et al.*, 2016); (b) North/South Waterway of Baimao Shoal (Yang, 2014); (c) North/South Channel (Yun, 2004; Wu, 2017); and (d) North/South Passage (Yun, 2004; Dao *et al.*, 2018). The symbols R, n, and P represent the correlation coefficient, the number of points, and the significance level of the linear regression. Relevant references are listed in the Supplementary Material.
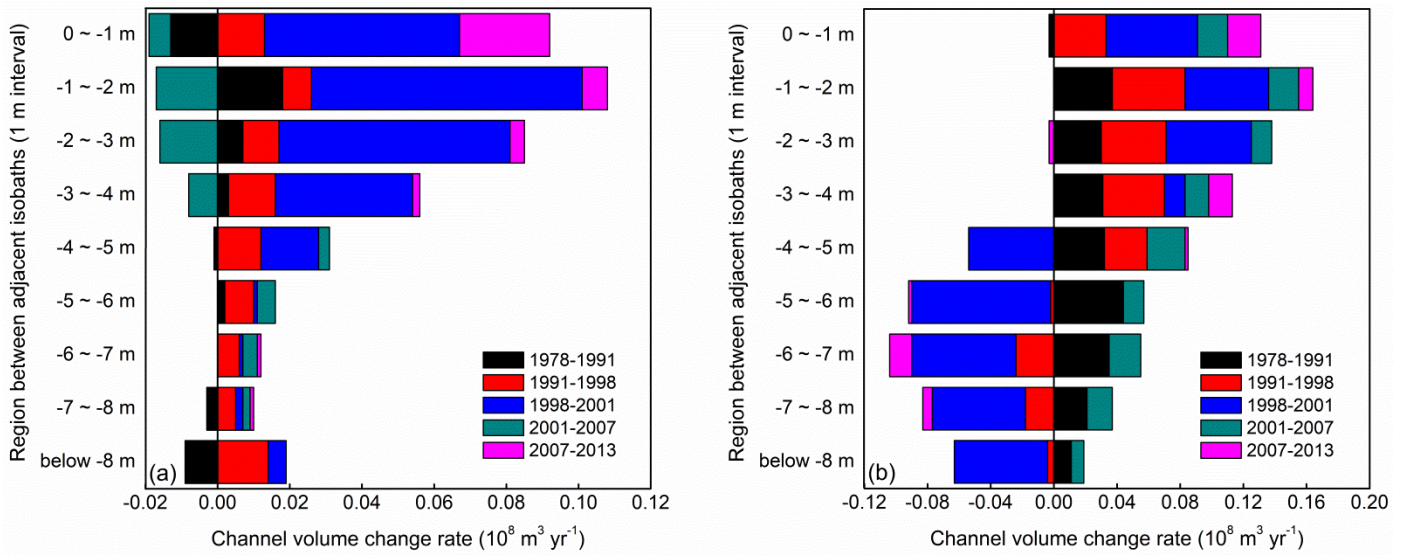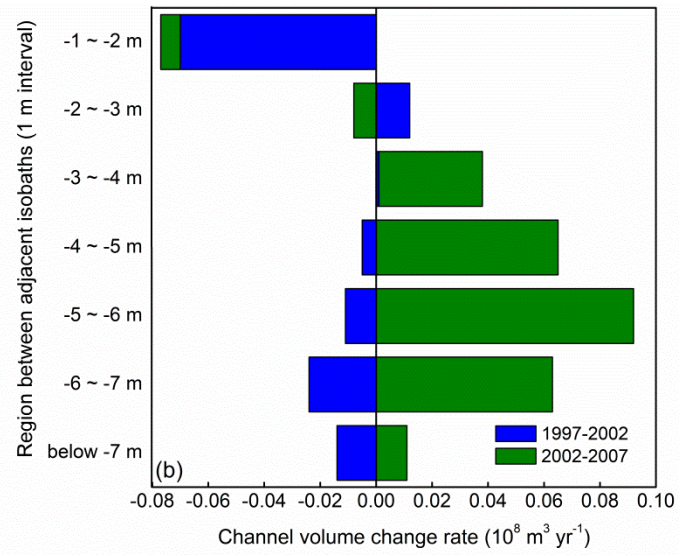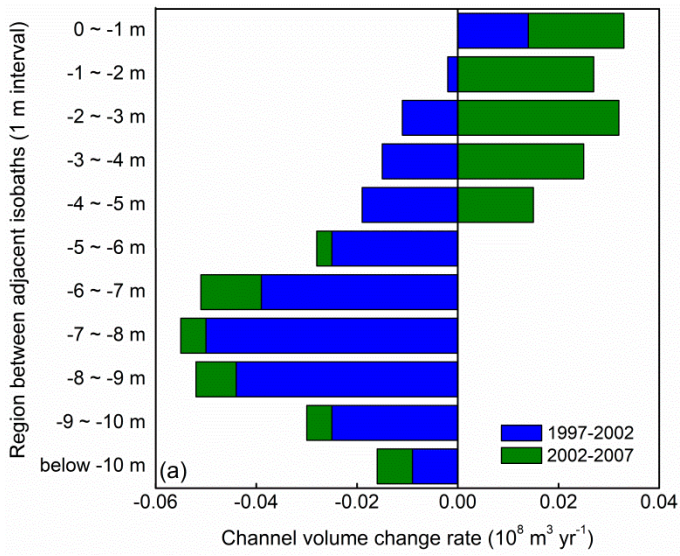
Figure 7. Channel volume change rates (deposition positive-valued, and erosion negative-valued) between adjacent isobaths (1 m interval) in (a) upper and (b) lower sub-reaches of the North Branch during different periods. Supplementary Figure S1 shows the boundaries of upper and lower sub-reaches of North Branch. Original data for this plot are listed in Supplementary Table SII, and were calculated using bed-elevation point data in Supplementary Table SI.

Figure 8. Channel volume change rates (deposition positive-valued, and erosion negative-valued) between adjacent isobaths (1 m interval) in (a) upper and (b) lower sub-reaches of the South Passage during different periods. Supplementary Figure S8 shows the boundaries of upper and lower sub-reaches of the South Passage. Original data for this plot are listed in Supplementary Table SIII, and were calculated using bed-elevation point data in Supplementary Table SI.

614

615

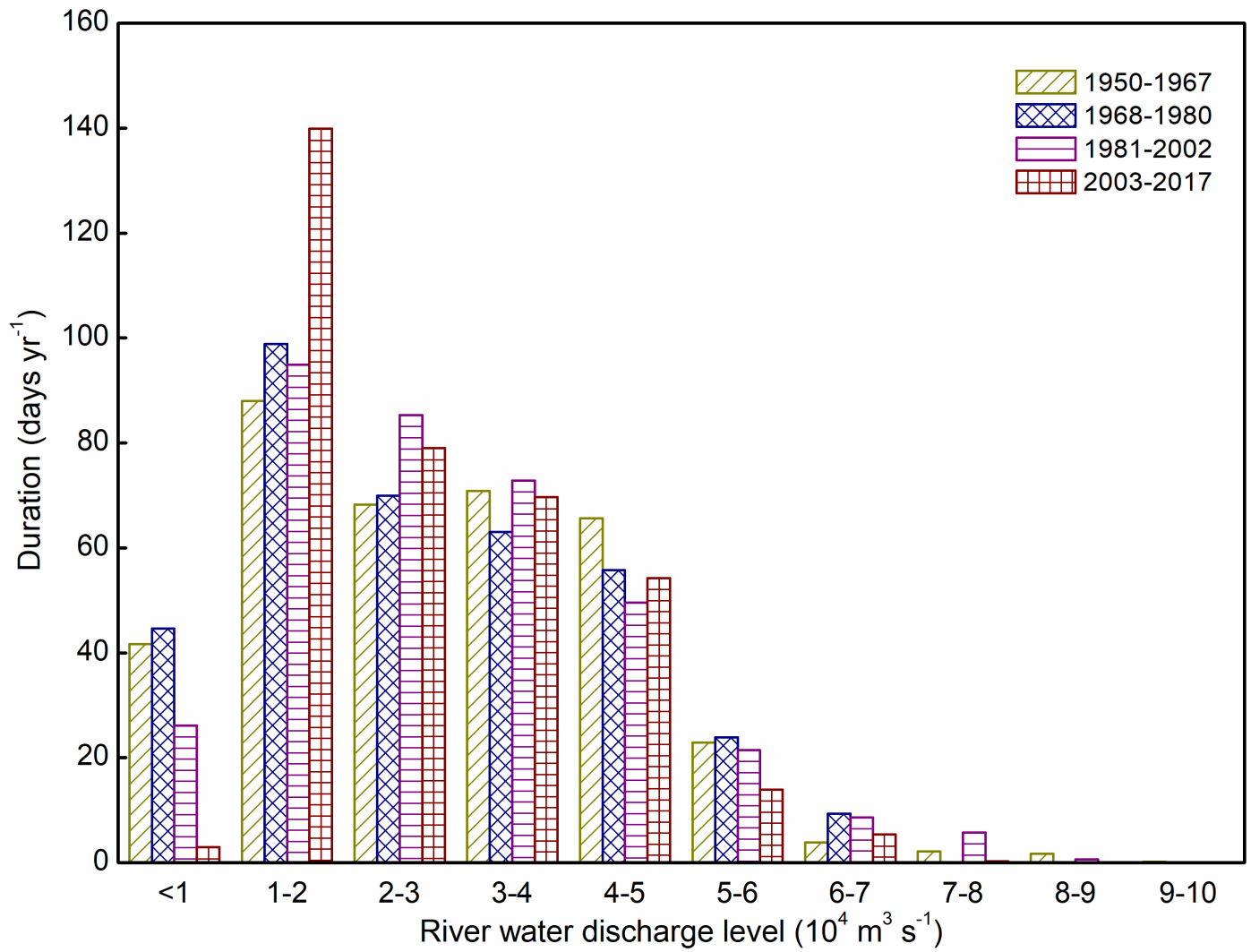616 **Figure 9.** Histogram of multi-year average duration days for different levels of runoff discharge at Datong based

617 on daily river water discharge series (see Supplementary Table SI) during the different construction stages of

618 major dams along the Yangtze River. The dividing years of 1968, 1981, and 2003 represent commencement of

619 impoundment of Danjiangkou Dam, Gezhou Dam, and the Three Gorges Dam (Figure 1a).

620
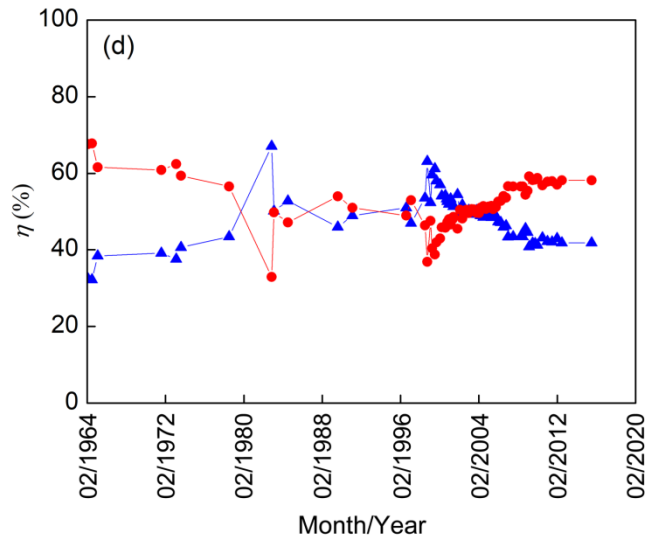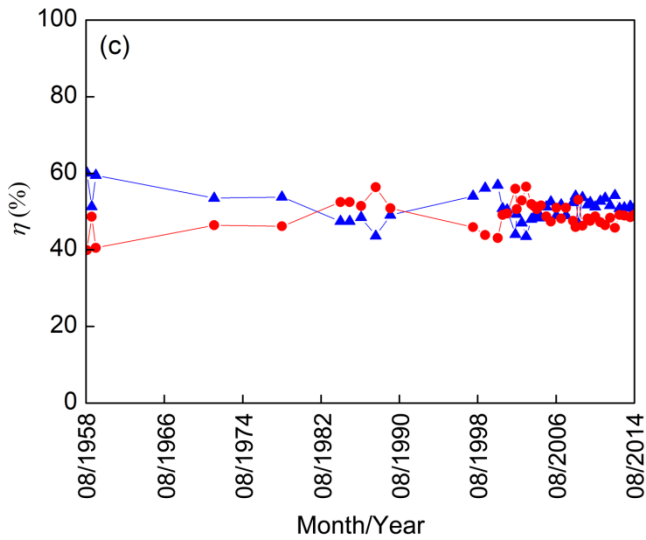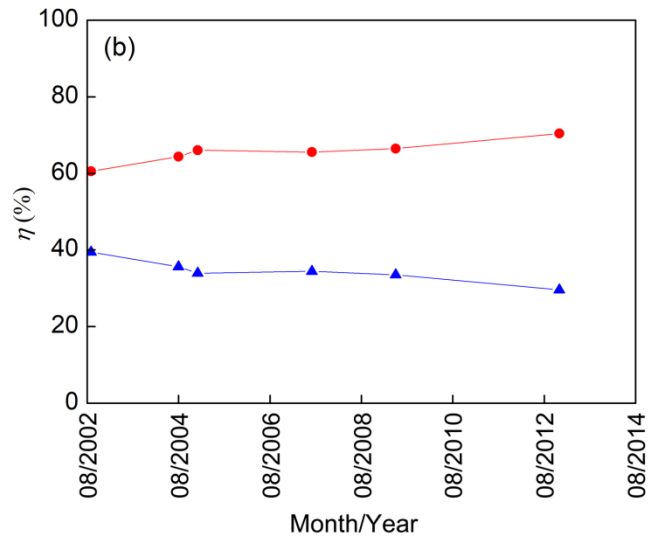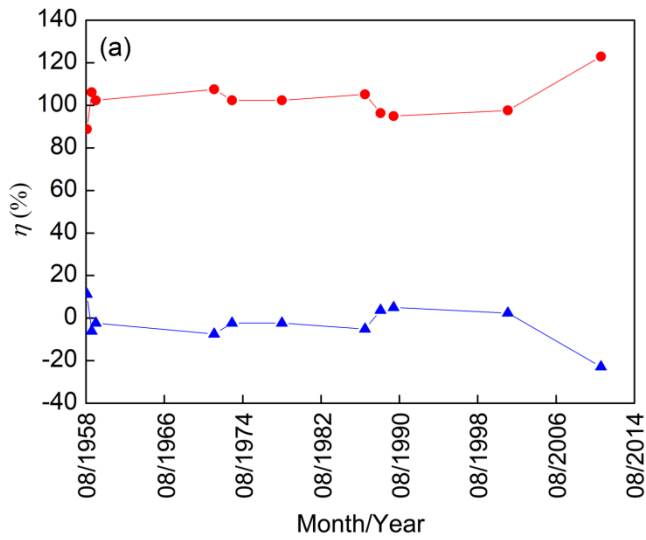
621   ▲ Situation for the north branching channel of each bifurcation   ● Situation for the south branching channel of each bifurcation

Figure 10. Time histories of ebb partition ratios for inland branching channels of the Yangtze Estuary: (a) North/South Branch (Dai *et al.*, 2016); (b) North/South Waterway of Baimao Shoal (Yang, 2014); (c) North/South Channel (Yun, 2004; Wu, 2017); and (d) North/South Passage (Yun, 2004; Dao *et al.*, 2018). Relevant references are listed in the Supplementary Material.
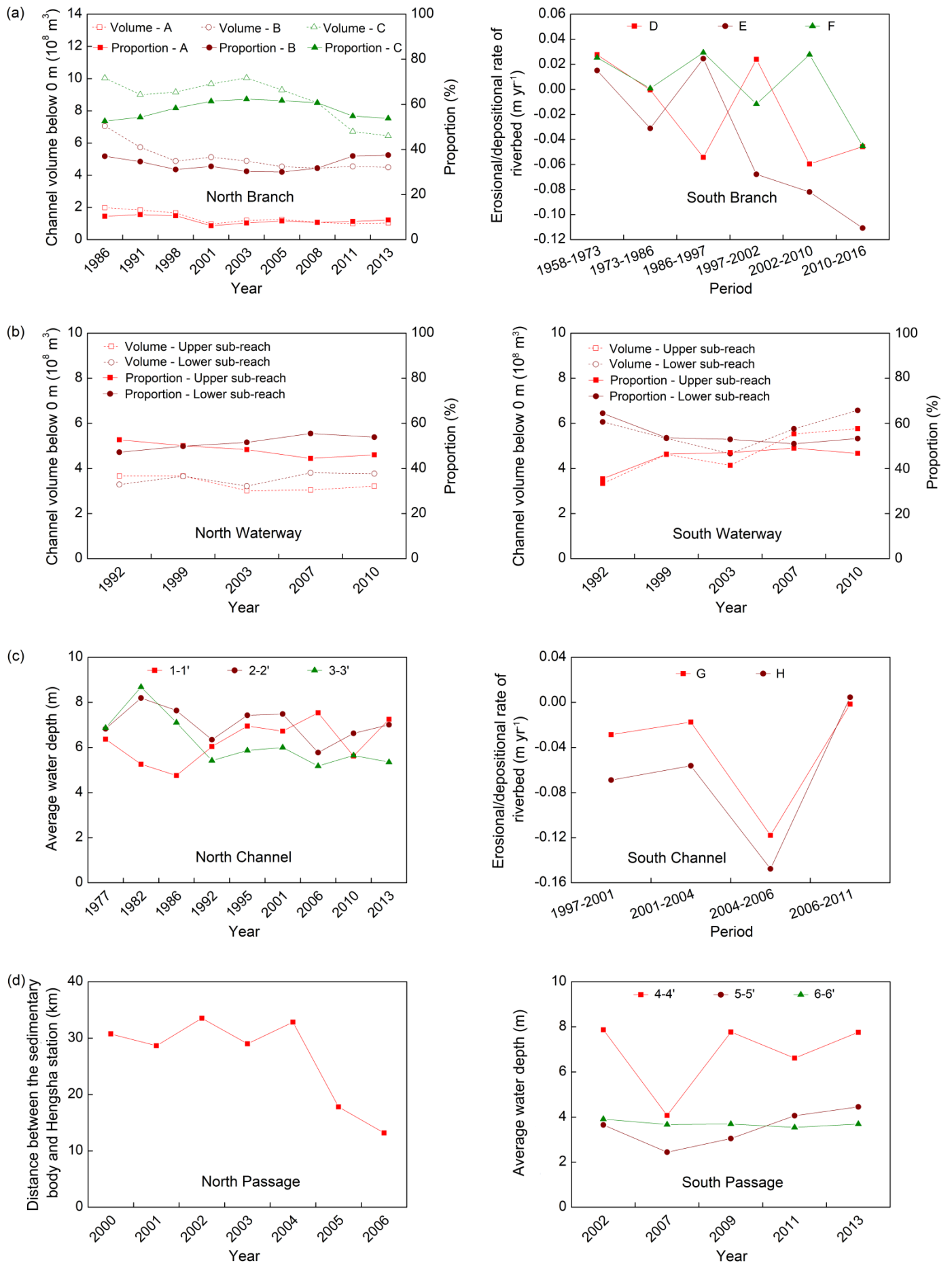
Figure 11. Time histories of indexes that characterize longitudinal morphological evolution within inland

branching channels in the Yangtze Estuary: (a) channel volume below the 0 m isobath for sub-reaches A, B and C

631   of the North Branch (Yang *et al*., 2016), and as proportions of total channel volume below the 0 m isobath, and

632   riverbed erosion/deposition rates for sub-reaches D, E and F of the South Branch (Zhao *et al*., 2018); (b) channel

633   volume below the 0 m isobath for upper and lower sub-reaches of the North/South Waterway of Baimao Shoal,

634   based on bed-elevation point data (Supplementary Table SI), and as proportions of total channel volume below

635   the 0 m isobath; (c) average water depth at cross-sections 1-1', 2-2' and 3-3' in North Channel (Guo *et al*., 2016a),

636   and riverbed erosion/deposition for sub-reaches G and H of the South Channel (Zhu and Luo, 2015); and (d)

637   distance between the sedimentary body in North Passage and Hengsha station (Liu *et al.*, 2009), and mean water

638   depth at cross-sections 4-4', 5-5' and 6-6' in the South Passage (Guo *et al.*, 2016b). Figure 1b and Figures S3-S4

639   indicate divisions among the sub-reaches in this plot and locations of cross-sections and Hengsha station.

640   Relevant references are listed in the Supplementary Material.

641

642

643 **Table I.** Riverbed erosion/deposition rates (deposition positive-valued, and erosion negative-valued) for

644 upper/lower sub-reaches, and multi-year average ebb partition ratios (η) within the inland branching channels in

645 the Yangtze Estuary over different periods and for corresponding multi-year average values of $D_{\geq 60,000}$.

Bifurcation	Branching channel	Period	Riverbed erosion/deposition rate (m yr^{-1}) [†]		η (%) [‡]	$D_{\geq 60,000}$ (days yr^{-1}) [§]
			Upper sub-reach	Lower sub-reach		
First bifurcation	North Branch	1978-1991	0.060	0.076	0.27	6
		1991-1998	0.094	0.038	3.66	26
		1998-2001	0.295	-0.089	3.66	36
		2001-2007	-0.018	0.046	-10.30	3
		2007-2013	0.020	-0.064	-10.30	5
	South Branch	1997-2002	-0.056	-0.019	96.34	29
		2002-2007	0.046	0.089	110.30	4
Second bifurcation	North Waterway of Baimao Shoal	1992-1999	0.234	-0.080		31
		1999-2003	0.210	0.108		15
		2003-2007	0.156	-0.157	35.81	0
		2007-2010	0.161	0.030	32.90	9
	South Waterway of Baimao Shoal	1992-1999	-0.282	0.424		31
		1999-2003	-0.330	0.103		15
		2003-2007	-0.228	-0.423	64.19	0
		2007-2010	-0.140	-0.263	67.10	9
Third bifurcation	North Channel	1997-2002	-0.070	-0.031	52.17	29
		2002-2007	0.116	0.119	49.12	4
	South Channel	1997-2002	-0.080	-0.114	47.83	29
		2002-2007	-0.033	-0.010	50.88	4
Fourth bifurcation	North Passage	1997-2002	-0.087	0.002	54.83	29
		2002-2006	0.310	0.026	49.14	4
		2006-2007	0.389	0.287	45.65	0
		2007-2009	-0.261	-0.275	43.30	0
	South Passage	1997-2002	-0.139	-0.006	45.17	29
		2002-2007	0.074	0.138	51.52	4

646 [†] Supplementary Figures S1-S8 indicate boundaries of upper and lower sub-reaches of the branching channels

647 for calculating riverbed erosion/deposition rates based on bed-elevation point data (Supplementary Table SI).

648 [‡] Data for calculating multi-year average ebb partition ratios in the branching channels were collected from

649 published literature listed in the References of the Supplementary Material, i.e. North/South Branch (Dai *et al.*,

650 2016), North/South Waterway of Baimao Shoal (Yang, 2014), North/South Channel (Wu, 2017) and North/South

651 Passage (Dao *et al.*, 2018).

652 [§] $D_{\geq 60,000}$ values were determined from daily river water discharge series (Supplementary Table SI).

Table II. Position of offshore depo-center and multi-year average ebb partition ratio (η) for inland branching channels in the Yangtze Estuary over different periods and for corresponding multi-year average values of $D_{\geq 60,000}$.

Period	Position of offshore depo-center [†]	Direction of movement of offshore depo-center	η (%) [‡]								$D_{\geq 60,000}$ (days yr^{-1}) [§]
			First bifurcation		Second bifurcation		Third bifurcation		Fourth bifurcation		
			North Branch	South Branch	North Waterway	South Waterway	North Channel	South Channel	North Passage	South Passage	
1958-1978	-10 m isobath seaward of opening of South Passage		-1.58	101.58			55.64	44.36	37.67	62.33	6
1978-1989	Area shallower than -10 m isobath along North Channel	Northward	-1.30	101.30			48.17	51.83	51.92	48.08	6
1989-1997	Area shallower than -10 m isobath off North Passage	Southward	3.65	96.35			51.10	48.90	48.22	51.78	13
1997-2002	Near opening of South Passage	Southward	3.66	96.34			52.17	47.83	54.83	45.17	29
2002-2004	Area deeper than -10 m isobath off opening of South Passage	Southeastward			37.58	62.42	46.62	53.38	50.07	49.93	7
2004-2007	Area deeper than -10 m isobath off opening of North Passage	Northward	-10.30	110.30	34.62	65.38	50.00	50.00	47.93	52.07	0
2007-2009	North channel in vicinity of -10m isobath	Northward			33.40	66.60	51.21	48.79	43.30	56.70	0
2009-2011	Near Hengsha East Shoal and opening of North Passage	Southward			31.60	68.40	52.09	47.91	41.95	58.05	12
2011-2013	No obvious offshore depo-center (significant erosion occurred in the whole Yangtze Estuary)				29.50	70.50	52.50	47.50	42.22	57.78	0
2013-2015	Near opening of North Channel	Northward					50.84	49.16	41.73	58.27	1

655   [†] Data on the depo-center position were obtained from Dai *et al*. (2014) and Chen *et al*. (2018), as listed in References of Supplementary Material.

656   [‡] Data for calculating multi-year average ebb partition ratios in the branching channels were collected from published literature listed in the References of the

657   Supplementary Material, i.e. North/South Branch (Dai *et al*., 2016), North/South Waterway of Baimao Shoal (Yang, 2014), North/South Channel (Yun, 2004; Wu, 2017)

658   and North/South Passage (Yun, 2004; Dao *et al*., 2018).

659   [§] $D_{\geq 60,000}$ values were determined from daily river water discharge series (Supplementary Table SI).

660 **Table III.** Roles of boundary change and sediment deposition in channel volume reduction below 0 m isobath of

661 North Branch during different periods.

Period	Reduction in channel volume below 0 m isobath (10^8 m^3) [†]			Contributing proportion (%)	
	Total reduction	Reduction caused by boundary change	Reduction caused by sediment deposition	Boundary change	Sediment deposition
1978-1991	3.128	1.274	1.854	40.73	59.27
1991-1998	1.592	0.787	0.805	49.43	50.57
1998-2001	0.324	0.285	0.039	87.96	12.04
2001-2007	0.685	0.295	0.390	43.07	56.93
2007-2013	0.379	0.514	-0.135 [‡]	135.61	-35.61

662 [†] Channel volume reduction calculated using bed-elevation point data (Supplementary Table SI).

663 [‡] Negative values related to sediment deposition during 2007-2013 indicate that river bed experienced erosion

664 causing an increase in channel volume of a certain reach in the North Branch during this period.

665

666

667 **Table IV.** Riverbed erosion/deposition rates (deposition positive-valued, and erosion negative-valued) in

668 upper/lower segment of the lower sub-reach of the North Branch over different periods and for corresponding

669 values of ebb partition ratio (η) and $D_{\geq 60,000}$.

Period	Riverbed erosion/deposition rate (m yr^{-1}) [†]		η (%) [‡]	$D_{\geq 60,000}$ (days yr^{-1}) [§]
	Upper segment	Lower segment		
1978-1991	0.051	0.093	0.27	6
1991-1998	0.050	0.030	3.66	26
1998-2001	-0.088	-0.089	3.66	36
2001-2007	0.074	0.032	-10.30	3
2007-2013	-0.026	-0.092	-10.30	5

670 [†] Supplementary Figure S1 shows the boundaries of upper and lower segments of the lower sub-reach of the

671 North Branch used in calculating riverbed erosion/deposition rates, based on bed-elevation point data

672 (Supplementary Table SI).

673 [‡] Data for calculating multi-year average ebb partition ratios in North Branch were obtained from Dai *et al*. (2016),

674 as listed in the References of the Supplementary Material.

675 [§] $D_{\geq 60,000}$ values were determined from daily river water discharge series (Supplementary Table SI).

676

677